Numerical and experimental investigation of light emissions of a planar nitrogen atmospheric-pressure dielectric barrier discharge due to addition of ammonia considering oxygen impurity

2013 Plasma Sources Sci. Technol. 22 065003

(http://iopscience.iop.org/0963-0252/22/6/065003)

Plasma Sources Sci. Technol. **22** (2013) 065003 (16pp) doi:10.1088/0963-0252/22/6/065003

Numerical and experimental investigation of light emissions of a planar nitrogen atmospheric-pressure dielectric barrier discharge due to addition of ammonia considering oxygen impurity

F-L Li[1], C-T Hung[1], K-M Lin[1], T-C Wei[2] and J-S Wu[1]

[1] Department of Mechanical Engineering, National Chiao Tung University, Hsinchu, Taiwan
[2] Department of Chemical Engineering, Chung Yuan Christian University, Taoyuan, Taiwan

E-mail: chongsin@faculty.nctu.edu.tw (J-S Wu)

Received 21 April 2013, in final form 8 August 2013
Published 8 October 2013
Online at stacks.iop.org/PSST/22/065003

Abstract

In this paper, the mechanisms of light emissions, including NO-γ, NO-β and N_2-SPS, produced in a N_2/NH_3 atmospheric-pressure dielectric barrier discharge considering realistic oxygen impurity (30 ppm) are investigated numerically and experimentally. Self-consistent, one-dimensional fluid modeling is used to numerically simulate the discharge process with 48 species and 235 reaction channels. An optical emission spectrometer (OES) is used to measure the relative intensities of the light emission. The simulations of the light emission intensities for the above-mentioned OES lines generally reproduce the trends observed in the experiments caused by changes in the NH_3 concentration. All of the predicted intensities of NO-γ, NO-β and N_2-SPS decrease with increasing amount of NH_3 caused by various reaction mechanisms. The former is due to the loss of $N_2(A)$ and NO(A) by the reaction of NH_3 with $N_2(A)$ and NO(A), respectively. The decrease in NO-β is due to the depletion of N and O because of NH_3, and the decrease in N_2-SPS is due to electron attachment to NH_3 and a weaker metastable–metastable associative ionization of N_2. All of the simulated results demonstrate that the discharges are typically Townsend-like because the ions outnumber the electrons and the electric field across the gap is distorted only slightly by the charged particles during the breakdown. Finally, a reduced chemical kinetics model for a planar atmospheric-pressure $N_2/O_2/NH_3$ dielectric barrier discharge is proposed and validated by benchmarking against the above complete chemical kinetics. This results in a reduced chemical kinetics consisting of 33 species and 87 reactions with a very limited loss of accuracy of discharge properties, while it is 2.1 times faster in computational time as compared with the complete version.

(Some figures may appear in colour only in the online journal)

1. Introduction

Nitrogen/ammonia atmospheric-pressure dielectric barrier discharges (AP-DBDs) have recently been used in enhancing the biocompatibility of PLA (polylactide) surfaces [1, 2] or LDPE (low-density polyethylene) [3]. Experiments [1–3] and numerical investigations [4] have been performed to understand the discharge physics and chemistry to some extent. However, the mechanisms of important light emission and the effects of oxygen impurities were not explored in these studies. These factors are important to gain a better understanding of the complex plasma chemistry and the interaction of light emission with the polymer surfaces that are treated.

Li *et al* [4] performed detailed one-dimensional (1D) fluid modeling of N_2/NH_3 AP-DBDs without including a detailed mechanism of light emissions (NO-γ, NO-β and N_2-SPS). The authors combined all of the excited/metastable nitrogen species into lumped excited nitrogen, and oxygen impurity was not considered in the modeling. We are especially interested in these three emission bands because they are often detected in a nitrogen-based discharge. In a commercial nitrogen bottle (e.g. 99.99%), we found that the oxygen impurity level could reach 30 ppm, based on measurements using a gas chromatographer (YL 6100GC, Young Lin Instrument Co., Ltd). Therefore, for realistic modeling of N_2/NH_3 AP-DBDs, the trace oxygen impurity level must be included to reproduce these light emissions.

Multidimensional fluid modeling for atmospheric-pressure plasmas using very complex plasma chemistry is generally very time-consuming and unnecessary for some applications. Thus, reduced chemical kinetics is often required to make the modeling more practical. In general, there are three reduction methods in the study of classical chemical kinetics [5]: reduction of the number of reacting species and reactions; reduced mechanism using quasi-steady-state and partial equilibrium assumptions; and mathematical representation based on the timescale separation. Chemkin [6] has often been used to reduce the number of reactions and species in a classical chemical mechanism without involving gas discharges. However, the simulated results using the Plasma PSR module of Chemkin (global modeling) are not compatible with the simulated results using fluid modeling (e.g. 1D), even with the same plasma chemistry, because the applied voltage, the driving frequency, the density of species and the electron temperature as a function of time and space are not considered in the zero-dimensional (0D) Chemkin model. Therefore, a combination of fluid modeling and global modeling is required to truly reproduce major discharge properties.

In this study, the optical emissions, including NO-γ, NO-β and N_2-SPS, generated in a planar N_2/NH_3 AP-DBD with trace levels of O_2 impurities were simulated using 1D self-consistent fluid modeling. The results are compared with the measurements obtained by an optical emission spectrometer (OES). A set of complex reaction pathways for the plasma chemistry of a planar $N_2/O_2/NH_3$ AP-DBD (48 species and 235 reactions) was developed to describe the discharge and the mechanism of light emissions generated by the gas discharge. The results of the trends of the simulated light intensities are in reasonable agreement with the experimental findings. The effect of ammonia addition into the N_2/O_2 discharge on the light intensities of the various emissions is presented and discussed in detail. Finally, we propose a general reduction method that can reduce the number of species and reactions by combining global modeling (e.g. Chemkin) with 1D fluid modeling with a minimal loss of accuracy. This method results in a reduced set of chemical kinetics (33 species and 87 reactions) for the 1D fluid model. This reduced chemistry is justified by the good agreement of the simulated discharge properties with the simulated properties obtained using a more complete set of chemistry (48 species and 235 reactions).

2. Numerical method

2.1. Fluid modeling

To simulate the complicated AP discharge physics and chemistry, a 1D fluid modeling was employed. We solved a set of model equations self-consistently that included the continuity equations for the charged species with a drift–diffusion approximation for the momentum equations, the neutral species continuity equations, the electron energy density equations and the Poisson equations [7]. The collocated cell-centered finite-volume method was used to discretize these equations. The discretized equations were solved by the semi-implicit method self-consistently at each time step. The corresponding numerical schemes and algorithms are described elsewhere in detail [7]. In addition, the transport coefficients and the rate constants related to the electrons are calculated by solving the Boltzmann equation using BOLSIG$^+$ [8]. Note that these coefficients were predicted in advance and stored in a lookup table as a function of the electron temperature with a gas temperature of 400 K. The mobilities of the ions are taken from the literature [9–11], and the corresponding diffusivities are calculated using the Einstein relation. The diffusivities of the neutral species are calculated from the Chapman–Enskog equation for binary diffusion [12]. The diffusivities of excited neutral species are assumed to be equal to those of the corresponding ground-state neutral species.

2.2. Plasma chemistry

In this study, a set of more complete plasma chemistry of an $N_2/O_2/NH_3$ discharge is first proposed, including 48 species (e^-, H^+, H_2^+, H_3^+, N^+, N_2^+, N_4^+, NH^+, NH_2^+, NH_3^+, NH_4^+, O_2^+, H^-, O^-, O_2^-, $N(^2D)$, $N(^2P)$, $N_2(A\,^3\Sigma_u^+)$, $N_2(B\,^3\Pi_g)$, $N_2(a'\,^1\Sigma_u^-)$, $N_2(C\,^3\Pi_u)$, $O(^1S)$, $O(^1D)$, $O_2(a)$, $O(^1S)N_2$, NO(A), NO(B), H, H_2, H_2O, H_2O_2, HNO, N, N_2, NH, NH_2, NH_3, N_2H, N_2H_2, N_2H_3, N_2H_4, NO, N_2O, NO_2, O, O_2, O_3 and OH) and 235 reaction channels, which are summarized in table 1, providing an extensive consideration of the complexity of the related chemical processes. The 235 reaction channels include 37 electron–molecular reactions, 5 electron–ion reactions, 37 positive ion–molecular reactions, 15 negative ion–molecular reactions, 10 positive ion–negative ion reactions, 124 neutral–neutral reactions and 7 excited species radiation reactions. Physically, this set of nitrogen/oxygen/ammonia plasma chemistry includes momentum transfer collision; electron-impact electronic excitation; electron-impact ionization; electron-impact dissociation; electron-impact dissociative ionization; electron-impact attachment; electron–ion dissociation; electron–ion dissociation from the ground state into an excited state; electron–ion dissociative recombination; positive ion–molecular charge exchange; negative ion–molecular detachment; positive ion–negative ion dissociation; positive ion–negative ion dissociative recombination; metastable–metastable associative ionization; excited/metastable–molecular excitation into an excited or metastable state; excited/metastable–molecular

Table 1. Summary of $N_2/O_2/NH_3$ plasma chemistry.

No	Reaction	Rate coefficient[a,b]	Threshold (eV)	Note[c]	Ref.
(1)	$e + N \rightarrow N + e$	BOLSIG$^+$	0.0		[29]
(2)	$e + N \rightarrow N(^2D) + e$	BOLSIG$^+$	2.38		[29]
(3)	$e + N \rightarrow N(^2P) + e$	BOLSIG$^+$	3.58		[29]
(4)	$e + N \rightarrow N^+ + 2e$	BOLSIG$^+$	14.54		[29]
(5)	$e + N_2 \rightarrow N_2 + e$	BOLSIG$^+$	0.0	S1, S2	[11]
(6)	$e + N_2 \rightarrow N_2(A\,^3\Sigma_u^+) + e$	BOLSIG$^+$	6.17	S1, S2	[11]
(7)	$e + N_2 \rightarrow N_2(B\,^3\Pi_g) + e$	BOLSIG$^+$	7.35	S1, S2	[11]
(8)	$e + N_2 \rightarrow N_2(a'\,^1\Sigma_u^-) + e$	BOLSIG$^+$	8.40	S1, S2	[11]
(9)	$e + N_2 \rightarrow N_2(C\,^3\Pi_u) + e$	BOLSIG$^+$	11.03	S1, S2	[11]
(10)	$e + N_2 \rightarrow N + N + e$	BOLSIG$^+$	13.0	S1, S2	[29]
(11)	$e + N_2 \rightarrow N_2^+ + 2e$	BOLSIG$^+$	15.58	S1, S2	[11]
(12)	$e + O_2 \rightarrow O_2 + e$	BOLSIG$^+$	0.0	S1, S2	[11]
(13)	$e + O_2 \rightarrow O^- + O$	BOLSIG$^+$	0.0		[11]
(14)	$e + O_2 + O_2 \rightarrow O_2^- + O_2$	BOLSIG$^+$	0.0	S1, S2	[11]
(15)	$e + O_2 \rightarrow O_2(a) + e$	BOLSIG$^+$	0.977		[11]
(16)	$e + O_2 \rightarrow 2O + e$	BOLSIG$^+$	6.0		[11]
(17)	$e + O_2 \rightarrow O + O(^1D) + e$	BOLSIG$^+$	8.4	S2	[11]
(18)	$e + O_2 \rightarrow O + O(^1S) + e$	BOLSIG$^+$	10.0		[11]
(19)	$e + O_2 \rightarrow O_2^+ + 2e$	BOLSIG$^+$	12.06		[11]
(20)	$e + O_3 \rightarrow e + O + O_2$	5.88×10^{-15}	0.0		[30]
(21)	$e + NH_3 \rightarrow NH_3 + e$	BOLSIG$^+$	0.0	S1, S2	[29]
(22)	$e + NH_3 \rightarrow NH_2 + H^-$	BOLSIG$^+$	0.0	S1, S2	[31]
(23)	$e + NH_3 \rightarrow NH_2 + H + e$	BOLSIG$^+$	5.72	S1, S2	[29]
(24)	$e + NH_3 \rightarrow NH + H + H + 2e$	BOLSIG$^+$	8.65		[29]
(25)	$e + NH_3 \rightarrow NH_3^+ + 2e$	BOLSIG$^+$	10.2	S1, S2	[29]
(26)	$e + NH_3 \rightarrow NH_2^+ + H + 2e$	BOLSIG$^+$	16.0	S1, S2	[29]
(27)	$e + NH_2 \rightarrow NH_2 + e$	BOLSIG$^+$	0.0		[29]
(28)	$e + NH_2 \rightarrow NH + H + e$	BOLSIG$^+$	5.72		[29]
(29)	$e + NH_2 \rightarrow N + H + H + 2e$	BOLSIG$^+$	8.65		[29]
(30)	$e + NH_2 \rightarrow NH_2^+ + 2e$	BOLSIG$^+$	11.14		[29]
(31)	$e + NH_2 \rightarrow NH^+ + H + 2e$	BOLSIG$^+$	17.6		[29]
(32)	$e + NH \rightarrow NH + e$	BOLSIG$^+$	0.0		[29]
(33)	$e + NH \rightarrow N + H + e$	BOLSIG$^+$	5.72		[29]
(34)	$e + NH \rightarrow NH^+ + 2e$	BOLSIG$^+$	13.49		[29]
(35)	$e + H_2 \rightarrow H_2 + e$	BOLSIG$^+$	0.0		[29]
(36)	$e + H_2 \rightarrow H + H + e$	BOLSIG$^+$	8.9		[29]
(37)	$e + H_2 \rightarrow H_2^+ + 2e$	BOLSIG$^+$	15.43		[29]
(38)	$e + N_2^+ \rightarrow N(^2D) + N$	3.7×10^{-13}	0.0		[11]
(39)	$e + N_2^+ \rightarrow 2N$	$2.8 \times 10^{-13} \left(T_g/T_e\right)^{0.5}$	0.0		[20]
(40)	$e + N_4^+ \rightarrow N_2(C\,^3\Pi_u) + N_2$	$2.0 \times 10^{-12} \left(T_g/T_e\right)^{0.5}$	0.0		[20]
(41)	$e + O_2^+ \rightarrow O(^1D) + O$	2.1×10^{-13}	0.0		[11]
(42)	$e + NH_4^+ \rightarrow NH_3 + H$	$9.0 \times 10^{-13} T_e^{-0.6}$	0.0		[18]
(43)	$N^+ + H_2 \rightarrow H_2^+ + N$	2.0×10^{-16}	0.0		[32]
(44)	$N^+ + NH_3 \rightarrow NH_3^+ + N$	1.7×10^{-15}	0.0		[32]
(45)	$N_2^+ + N \rightarrow N^+ + N_2$	5.0×10^{-18}	0.0		[29]
(46)	$N_2^+ + N_2 + N_2 \rightarrow N_4^+ + N_2$	1.0×10^{-44}	0.0	S1, S2	[33]
(47)	$N_2^+ + NH_3 \rightarrow NH_3^+ + N_2$	1.95×10^{-15}	0.0	S1, S2	[32]
(48)	$N_2^+ + H \rightarrow H^+ + N_2$	2.5×10^{-16}	0.0		[32]
(49)	$N_2^+ + H_2 \rightarrow H_2^+ + N_2$	4.0×10^{-16}	0.0		[32]
(50)	$N_4^+ + N \rightarrow N^+ + 2N_2$	1.0×10^{-17}	0.0		[33]
(51)	$N_4^+ + N_2 \rightarrow N_2^+ + 2N_2$	$2.1 \times 10^{-22} \exp(T_g/120)$	0.0	S1, S2	[34]
(52)	$N_4^+ + NH_3 \rightarrow NH_3^+ + 2N_2$	3.0×10^{-17}	0.0	S1, S2	[35]
(53)	$N_4^+ + H_2 \rightarrow H_2^+ + 2N_2$	$3 \times 10^{-16} \exp(-1800/T_g)$	0.0		[33]
(54)	$O_2^+ + NH_3 \rightarrow NH_3^+ + O_2$	1.0×10^{-15}	0.0		[36]
(55)	$NH^+ + NH_3 \rightarrow NH_4^+ + N$	1.8×10^{-15}	0.0		[29]
(56)	$NH^+ + H_2 \rightarrow NH_2^+ + H$	1.0×10^{-15}	0.0		[29]
(57)	$NH_2^+ + NH_3 \rightarrow NH_3^+ + NH_2$	2.2×10^{-15}	0.0	S1, S2	[29]
(58)	$NH_2^+ + NH_3 \rightarrow NH_4^+ + NH$	2.2×10^{-15}	0.0	S1, S2	[29]
(59)	$NH_2^+ + H_2 \rightarrow NH_3^+ + H$	1.0×10^{-15}	0.0	S1, S2	[29]
(60)	$NH_3^+ + NH_3 \rightarrow NH_2^+ + H_2 + NH_2$	6.12×10^{-13} $(T_g/298)^{-0.44} \exp(-3.8/T_g)$	0.0	S1, S2	[29]
(61)	$NH_3^+ + NH_3 \rightarrow NH_4^+ + NH_2$	2.2×10^{-15}	0.0		[29]
(62)	$NH_3^+ + NH_3 \rightarrow H^+ + NH_2 + NH_3$	6.87×10^{-16} $(T_g/298)^{-0.17} \exp(-4.6/T_g)$	0.0		[29]

Table 1. (Continued.)

No	Reaction	Rate coefficient[a,b]	Threshold (eV)	Note[c]	Ref.
(63)	$NH_3^+ + H_2 \rightarrow NH_4^+ + H$	4.0×10^{-19}	0.0		[29]
(64)	$NH_3^+ + H_2 \rightarrow H^+ + NH_3 + H$	8.46×10^{-16} $(T_g/298)^{-0.39} \exp(-14.8/T_g)$	0.0		[29]
(65)	$NH_3^+ + H_2 \rightarrow H_2^+ + NH_3$	9.63×10^{-19} $(T_g/298)^{-0.25} \exp(-14.6/T_g)$	0.0		[29]
(66)	$NH_3^+ + H_2 \rightarrow H_2^+ + NH_2 + H$	2.18×10^{-15} $(T_g/298)^{-0.2} \exp(-9.9/T_g)$	0.0		[29]
(67)	$H^+ + NH_3 \rightarrow NH_3^+ + H$	5.0×10^{-17}	0.0		[29]
(68)	$H^+ + NH_2 \rightarrow NH_2^+ + H$	5.0×10^{-17}	0.0		[29]
(69)	$H^+ + NH \rightarrow NH^+ + H$	5.0×10^{-17}	0.0		[29]
(70)	$H^+ + H_2 \rightarrow H_2^+ + H$	$3.22 \times 10^{-16} \exp(21\,856/T_g)$	0.0		[29]
(71)	$H_2^+ + NH_3 \rightarrow NH_3^+ + H_2$	5.7×10^{-15}	0.0		[29]
(72)	$H_2^+ + NH_3 \rightarrow NH_4^+ + H$	5.0×10^{-17}	0.0		[29]
(73)	$H_2^+ + NH_2 \rightarrow NH_2^+ + H_2$	5.0×10^{-16}	0.0		[29]
(74)	$H_2^+ + NH_2 \rightarrow NH_3^+ + H$	5.0×10^{-17}	0.0		[29]
(75)	$H_2^+ + NH \rightarrow NH^+ + H_2$	5.0×10^{-16}	0.0		[29]
(76)	$H_2^+ + NH \rightarrow NH_2^+ + H$	5.0×10^{-17}	0.0		[29]
(77)	$H_2^+ + H \rightarrow H^+ + H_2$	6.40×10^{-16}	0.0		[29]
(78)	$H_2^+ + H_2 \rightarrow H_3^+ + H$	2.1×10^{-15}	0.0		[33]
(79)	$H_3^+ + NH_3 \rightarrow NH_4^+ + H_2$	4.4×10^{-15}	0.0		[29]
(80)	$O_2^- + N \rightarrow NO_2 + e$	5.0×10^{-16}	0.0		[37]
(81)	$O_2^- + N_2(A\,^3\Sigma_u^+) \rightarrow O_2 + N_2 + e$	2.1×10^{-15}	0.0	S1, S2	[11]
(82)	$O_2^- + N_2(B\,^3\Pi_g) \rightarrow O_2 + N_2 + e$	2.5×10^{-15}	0.0		[38]
(83)	$O_2^- + O \rightarrow O_3 + e$	1.5×10^{-16}	0.0		[11]
(84)	$O_2^- + O_2(a) \rightarrow 2O_2 + e$	2.0×10^{-16}	0.0		[11]
(85)	$O_2^- + H_2 \rightarrow H_2O_2 + e$	1.0×10^{-15}	0.0		[32]
(86)	$O^- + N \rightarrow NO + e$	2.6×10^{-16}	0.0		[11]
(87)	$O^- + N_2(A\,^3\Sigma_u^+) \rightarrow O + N_2 + e$	2.2×10^{-15}	0.0		[11]
(88)	$O^- + N_2(B\,^3\Pi_g) \rightarrow O + N_2 + e$	1.9×10^{-15}	0.0		[38]
(89)	$O^- + O \rightarrow O_2 + e$	5.0×10^{-16}	0.0		[11]
(90)	$O^- + O_2 \rightarrow O_3 + e$	5.0×10^{-21}	0.0		[38]
(91)	$O^- + O_2(a) \rightarrow O_3 + e$	3.0×10^{-16}	0.0		[38]
(92)	$O^- + NO \rightarrow NO_2 + e$	2.6×10^{-16}	0.0		[37]
(93)	$O^- + H_2O \rightarrow H_2O_2 + e$	6.0×10^{-19}	0.0		[30]
(94)	$H^- + H \rightarrow H_2 + e$	1.8×10^{-15}	0.0	S1, S2	[18]
(95)	$N_2^+ + O^- \rightarrow N_2 + O$	7.8×10^{-12}	0.0		[11]
(96)	$N_4^+ + O_2^- \rightarrow N_2 + N_2 + O_2$	$2.0 \times 10^{-12}(T_g/300)^{-0.5}$	0.0	S1, S2	[36]
(97)	$O_2^+ + O^- \rightarrow O_2 + O$	7.5×10^{-12}	0.0		[11]
(98)	$O_2^+ + O_2^- \rightarrow 2O_2$	7.8×10^{-12}	0.0		[11]
(99)	$NH_3^+ + O^- \rightarrow NH_3 + O$	$3.0 \times 10^{-12}(T_g/300)^{-0.5}$	0.0		[36]
(100)	$NH_3^+ + O_2^- \rightarrow NH_3 + O_2$	$2.0 \times 10^{-12}(T_g/300)^{-0.5}$	0.0		[36]
(101)	$NH_4^+ + O^- \rightarrow NH_3 + OH$	$3.0 \times 10^{-12}(T_g/300)^{-0.5}$	0.0		[36]
(102)	$NH_4^+ + O_2^- \rightarrow NH_3 + H + O_2$	$2.0 \times 10^{-12}(T_g/300)^{-0.5}$	0.0	S1, S2	[36]
(103)	$H^- + N_2^+ \rightarrow H + N_2$	$3.0 \times 10^{-12}(T_g/300)^{-0.5}$	0.0		[36]
(104)	$H^- + N_4^+ \rightarrow H + 2N_2$	1.5×10^{-13}	0.0	S1, S2	[34]
(105)	$N_2(A\,^3\Sigma_u^+) + N_2(A\,^3\Sigma_u^+) \rightarrow N_2 + N_2(B\,^3\Pi_g)$	7.7×10^{-19}	0.0		[20]
(106)	$N_2(A\,^3\Sigma_u^+) + N_2(A\,^3\Sigma_u^+) \rightarrow N_2 + N_2(C\,^3\Pi_u)$	3.0×10^{-16}	0.0	S1, S2	[20]
(107)	$N_2(A\,^3\Sigma_u^+) + O \rightarrow N(^2D) + NO$	7.0×10^{-19}	0.0		[11]
(108)	$N_2(A\,^3\Sigma_u^+) + O \rightarrow O(^1S) + N_2$	2.1×10^{-17}	0.0	S1, S2	[38]
(109)	$N_2(A\,^3\Sigma_u^+) + O_2 \rightarrow 2O + N_2$	1.7×10^{-18}	0.0	S1, S2	[11]
(110)	$N_2(A\,^3\Sigma_u^+) + O_2 \rightarrow O_2(a) + N_2$	7.5×10^{-19}	0.0	S1, S2	[11]
(111)	$N_2(A\,^3\Sigma_u^+) + NO \rightarrow NO(A) + N_2$	6.6×10^{-17}	0.0	S1, S2	[39]
(112)	$N_2(A\,^3\Sigma_u^+) + NH_3 \rightarrow N_2 + NH_2 + H$	3.0×10^{-19}	0.0	S1, S2	[40]
(113)	$N_2(A\,^3\Sigma_u^+) + NH_3 \rightarrow N_2 + NH + H_2$	1.0×10^{-19}	0.0	S1, S2	[32]
(114)	$N_2(A\,^3\Sigma_u^+) + NH_2 \rightarrow N_2 + NH + H$	1.6×10^{-17}	0.0	S1, S2	[32]
(115)	$N_2(A\,^3\Sigma_u^+) + H_2 \rightarrow N_2 + 2H$	$2.0 \times 10^{-16} \exp(-3500/T_g)$	0.0		[33]
(116)	$N_2(B\,^3\Pi_g) + N_2 \rightarrow N_2(A\,^3\Sigma_u^+) + N_2$	3.0×10^{-17}	0.0	S1, S2	[11]
(117)	$N_2(B\,^3\Pi_g) + O_2 \rightarrow 2O + N_2$	1.1×10^{-16}	0.0		[11]
(118)	$N_2(B\,^3\Pi_g) + H_2 \rightarrow N_2(A\,^3\Sigma_u^+) + H_2$	2.5×10^{-17}	0.0		[33]
(119)	$N_2(a'\,^1\Sigma_u^-) + N_2(A\,^3\Sigma_u^+) \rightarrow N_4^+ + e$	5.0×10^{-17}	0.0	S1, S2	[38]
(120)	$N_2(a'\,^1\Sigma_u^-) + N_2(a'\,^1\Sigma_u^-) \rightarrow N_4^+ + e$	2.0×10^{-16}	0.0	S1, S2	[38]
(121)	$N_2(a'\,^1\Sigma_u^-) + N_2 \rightarrow N_2(B\,^3\Pi_g) + N_2$	2.0×10^{-19}	0.0	S1, S2	[20]
(122)	$N_2(a'\,^1\Sigma_u^-) + N_2 \rightarrow 2N_2$	2.0×10^{-19}	0.0	S1, S2	[20]

Table 1. (Continued.)

No	Reaction	Rate coefficient[a,b]	Threshold (eV)	Note[c]	Ref.
(123)	$N_2(a'\,^1\Sigma_u^-) + O_2 \rightarrow 2O + N_2$	2.8×10^{-17}	0.0	S1, S2	[11]
(124)	$N_2(a'\,^1\Sigma_u^-) + NO \rightarrow O + N + N_2$	3.6×10^{-16}	0.0		[11]
(125)	$N_2(a'\,^1\Sigma_u^-) + H \rightarrow N_2 + H$	1.5×10^{-16}	0.0		[33]
(126)	$N_2(a'\,^1\Sigma_u^-) + H_2 \rightarrow N_2 + 2H$	2.6×10^{-17}	0.0		[33]
(127)	$N_2(C\,^3\Pi_u) + N_2 \rightarrow N_2(a'\,^1\Sigma_u^-) + N_2$	1.0×10^{-17}	0.0	S1, S2	[11]
(128)	$N_2(C\,^3\Pi_u) + O_2 \rightarrow N_2 + O + O(^1S)$	3.0×10^{-16}	0.0	S1, S2	[11]
(129)	$N(^2D) + O_2 \rightarrow NO + O$	$1.5 \times 10^{-18} \times (T_g/300)^{0.5}$	0.0		[38]
(130)	$N(^2D) + O_2 \rightarrow NO + O(^1D)$	6.0×10^{-18}	0.0		[11]
(131)	$N(^2D) + H_2 \rightarrow NH + H$	2.3×10^{-18}	0.0		[33]
(132)	$N(^2D) + NH_3 \rightarrow NH + NH_2$	1.1×10^{-16}	0.0		[33]
(133)	$N(^2D) + N_2O \rightarrow N_2 + NO$	3.61×10^{-18}	0.0		[41]
(134)	$N(^2P) + NH_3 \rightarrow NH + NH_2$	7.0×10^{-17}	0.0		[32]
(135)	$N(^2P) + H_2 \rightarrow H + NH$	2.5×10^{-20}	0.0		[33]
(136)	$O(^1S) + N_2 + N_2 \rightarrow O(^1S)N_2 + N_2$	2.0×10^{-48}	0.0	S2	[39]
(137)	$O(^1S) + H_2O \rightarrow OH + OH$	3.0×10^{-16}	0.0	S1, S2	[30]
(138)	$O(^1D) + O_2 \rightarrow O + O_2(a)$	3.4×10^{-17}	0.0	S2	[11]
(139)	$O(^1D) + O_2 \rightarrow O + O_2$	$6.4 \times 10^{-18}\exp(67/T_g)$	0.0		[38]
(140)	$O(^1D) + NH_3 \rightarrow NH + H_2O$	2.9×10^{-17}	0.0	S2	[32]
(141)	$O(^1D) + NH_3 \rightarrow OH + NH_2$	2.9×10^{-16}	0.0	S2	[32]
(142)	$O(^1D) + H_2 \rightarrow OH + H$	1.1×10^{-16}	0.0		[36]
(143)	$O(^1D) + H_2O \rightarrow OH + OH$	1.8×10^{-16}	0.0		[41]
(144)	$O(^1D) + H_2O_2 \rightarrow H_2O + O_2$	5.2×10^{-16}	0.0		[30]
(145)	$O_2(a) + NH_3 \rightarrow NH_3 + O_2$	8.92×10^{-24}	0.0		[41]
(146)	$O_2(a) + NH_2 \rightarrow HNO + OH$	1.0×10^{-20}	0.0		[32]
(147)	$O_2(a) + NH \rightarrow NO + OH$	1.0×10^{-20}	0.0		[32]
(148)	$NO(A\,^2\Sigma^+) + N_2 \rightarrow NO + N_2$	5.0×10^{-20}	0.0	S1, S2	[39]
(149)	$NO(A\,^2\Sigma^+) + O_2 \rightarrow NO + O_2$	1.5×10^{-16}	0.0		[42]
(150)	$NO(A\,^2\Sigma^+) + NH_3 \rightarrow NO + NH_3$	4.5×10^{-15}	0.0	S1, S2	[28]
(151)	$NO(B\,^2\Pi) + N_2 \rightarrow NO + N_2$	6.1×10^{-22}	0.0	S1, S2	[39]
(152)	$NO(B\,^2\Pi) + O_2 \rightarrow NO + O_2$	1.5×10^{-17}	0.0	S1, S2	[42]
(153)	$O(^1S)N_2 + N_2 \rightarrow O(^1S) + N_2 + N_2$	5.0×10^{-18}	0.0	S2	[39]
(154)	$O(^1S)N_2 + NH_3 \rightarrow O(^1S) + N_2 + NH_3$	5.0×10^{-18}	0.0		[28]
(155)	$N + N + NH_3 \rightarrow N_2 + NH_3$	1.0×10^{-44}	0.0		[29]
(156)	$N + O + N_2 \rightarrow NO(B\,^2\Pi) + N_2$	$(1/35) \times 1.76 \times 10^{-39} \times T_g^{-0.5}$	0.0	S1, S2	[42]
(157)	$N + O + NH_3 \rightarrow NO(B\,^2\Pi) + NH_3$	$(1/35) \times 1.76 \times 10^{-35} \times T_g^{-0.5}$	0.0	S1, S2	[42]
(158)	$N + O + N_2 \rightarrow NO + N_2$	$1.76 \times 10^{-42} T_g^{-0.5}$	0.0	S1, S2	[38]
(159)	$N + H + NH_3 \rightarrow NH + NH_3$	5.0×10^{-44}	0.0		[29]
(160)	$N + H + H \rightarrow NH + H$	5.0×10^{-44}	0.0		[29]
(161)	$N + H_2 \rightarrow NH + H$	$2.66 \times 10^{-16}\exp(-12\,609/T_g)$	0.0		[29]
(162)	$N_2 + N_2 \rightarrow N + N + N_2$	$4.29 \times 10^{-16}\exp(-86\,460/T_g)$	0.0		[29]
(163)	$O + O_2 + N_2 \rightarrow O_3 + N_2$	5.6×10^{-46}	0.0		[11]
(164)	$O + NH_3 \rightarrow OH + NH_2$	3.59×10^{-21}	0.0	S1, S2	[41]
(165)	$O + NH_2 \rightarrow H + HNO$	2.78×10^{-17}	0.0		[41]
(166)	$O + NH_2 \rightarrow OH + NH$	1.2×10^{-17}	0.0	S1, S2	[41]
(167)	$O + NH \rightarrow NO + H$	1.16×10^{-16}	0.0	S1, S2	[41]
(168)	$O + N_2H_2 \rightarrow NH_2 + NO$	1.66×10^{-17}	0.0	S1, S2	[32]
(169)	$O + N_2H_3 \rightarrow NH_2 + HNO$	1.66×10^{-17}	0.0	S1, S2	[32]
(170)	$O + N_2H_4 \rightarrow N_2H_3 + OH$	5×10^{-18}	0.0		[32]
(171)	$O + HNO \rightarrow OH + NO$	1.82×10^{-17}	0.0		[36]
(172)	$O_2 + NH_2 \rightarrow HNO + OH$	1.0×10^{-24}	0.0		[32]
(173)	$O_3 + H \rightarrow OH + O_2$	4.31×10^{-17}	0.0		[41]
(174)	$H + H + N_2 \rightarrow H_2 + N_2$	$1.9 \times 10^{-43}(T_g/298)^{-0.06}$	0.0	S1, S2	[29]
(175)	$H + H + NH_3 \rightarrow H_2 + NH_3$	1.40×10^{-43}	0.0		[29]
(176)	$H + H + NH_2 \rightarrow H_2 + NH_2$	1.40×10^{-43}	0.0		[29]
(177)	$H + NH_2 + NH_3 \rightarrow NH_3 + NH_3$	6.0×10^{-42}	0.0		[29]
(178)	$H + NH_2 + NH_2 \rightarrow NH_3 + NH_2$	6.0×10^{-42}	0.0		[29]
(179)	$H + NH_2 + H \rightarrow H + NH_3$	6.0×10^{-42}	0.0		[29]
(180)	$H + H_2O_2 \rightarrow H_2O + OH$	$4 \times 10^{-17}\exp(-2000/T_g)$	0.0		[30]
(181)	$NH_3 + H \rightarrow H_2 + NH_2$	$1.34 \times 10^{-16}\exp(-7352/T_g)$	0.0		[29]
(182)	$NH_3 + NH + N_2 \rightarrow N_2H_4 + N_2$	5.0×10^{-47}	0.0		[29]
(183)	$NH_2 + N \rightarrow N_2 + H + H$	1.2×10^{-16}	0.0	S1, S2	[29]
(184)	$NH_2 + NH_2 \rightarrow H_2 + N_2H_2$	8.31×10^{-17}	0.0	S1, S2	[29]
(185)	$NH_2 + NH_2 \rightarrow NH_3 + NH$	$8.31 \times 10^{-17}\exp(-5100/T_g)$	0.0		[29]

Table 1. (Continued.)

No	Reaction	Rate coefficient[a,b]	Threshold (eV)	Note[c]	Ref.
(186)	$NH_2 + NH \rightarrow H + N_2H_2$	$2.49 \times 10^{-15}(T_g/298)^{-0.5}$	0.0	S1, S2	[29]
(187)	$NH_2 + NH \rightarrow N_2H_3$	1.16×10^{-16}	0.0	S1, S2	[29]
(188)	$NH_2 + H + N_2 \rightarrow NH_3 + N_2$	6.06×10^{-42}	0.0	S1, S2	[29]
(189)	$NH_2 + H \rightarrow H_2 + NH$	4.81×10^{-18}	0.0		[29]
(190)	$NH_2 + H_2 \rightarrow H + NH_3$	$2.09 \times 10^{-18} \exp(-4277/T_g)$	0.0		[29]
(191)	$NH + N \rightarrow N_2 + H$	2.5×10^{-17}	0.0	S1, S2	[29]
(192)	$NH + NH \rightarrow N_2 + H + H$	1.16×10^{-15}	0.0	S1, S2	[29]
(193)	$NH + NH \rightarrow NH_2 + N$	1.4×10^{-20} $(T_g/298)^{2.89} \exp(1015/T_g)$	0.0		[29]
(194)	$NH + NH \rightarrow N_2H_2$	3.49×10^{-18}	0.0		[29]
(195)	$NH + H \rightarrow H_2 + N$	$5.98 \times 10^{-17} \exp(-166/T_g)$	0.0	S1, S2	[29]
(196)	$NH + H_2 \rightarrow H + NH_2$	$5.96 \times 10^{-17} \exp(-7782/T_g)$	0.0		[29]
(197)	$N_2H + NH_2 \rightarrow N_2 + NH_3$	8.31×10^{-17}	0.0	S1, S2	[29]
(198)	$N_2H + NH \rightarrow N_2 + NH_2$	8.31×10^{-17}	0.0	S1, S2	[29]
(199)	$N_2H + H \rightarrow N_2 + H_2$	$6.64 \times 10^{-17} \exp(-1531/T_g)$	0.0	S1, S2	[29]
(200)	$N_2H_2 + NH_2 \rightarrow N_2 + H + NH_3$	1.53×10^{-19} $(T_g/298)^{4.05} \exp(810.7/T_g)$	0.0		[29]
(201)	$N_2H_2 + NH_2 \rightarrow N_2H + NH_3$	$1.66 \times 10^{-17}\exp(-510/T_g)$	0.0	S1, S2	[29]
(202)	$N_2H_2 + NH \rightarrow N_2H + NH_2$	$1.66 \times 10^{-17} \exp(-510/T_g)$	0.0		[29]
(203)	$N_2H_2 + H \rightarrow N_2 + H + H_2$	4.53×10^{-19} $(T_g/298)^{2.63} \exp(115/T_g)$	0.0		[29]
(204)	$N_2H_2 + H \rightarrow N_2H + H_2$	$8.31 \times 10^{-17} \exp(-510/T_g)$	0.0	S1, S2	[29]
(205)	$N_2H_3 + H \rightarrow NH_2 + NH_2$	2.66×10^{-18}	0.0	S1, S2	[29]
(206)	$N_2H_3 + N_2H_3 \rightarrow NH_3 + NH_3 + N_2$	5.0×10^{-18}	0.0		[29]
(207)	$N_2H_3 + N_2H_3 \rightarrow N_2H_4 + N_2H_2$	2.0×10^{-17}	0.0	S1, S2	[29]
(208)	$N_2H_4 + N \rightarrow NH_2 + N_2H_2$	1.25×10^{-19}	0.0		[29]
(209)	$N_2H_4 + NH_2 \rightarrow NH_3 + N_2H_3$	5.15×10^{-19}	0.0		[29]
(210)	$N_2H_4 + H \rightarrow N_2H_3 + H_2$	$1.17 \times 10^{-19} \exp(-1260.5/T_g)$	0.0		[29]
(211)	$NO + N \rightarrow N_2 + O$	3.4×10^{-17}	0.0	S1, S2	[41]
(212)	$NO + O + N_2 \rightarrow NO_2 + N_2$	8.4×10^{-44}	0.0		[37]
(213)	$NO + NH_2 \rightarrow N_2 + H_2O$	1.2×10^{-17}	0.0	S1, S2	[41]
(214)	$NO + NH_2 \rightarrow N_2 + H + OH$	1.7×10^{-18}	0.0	S1, S2	[43]
(215)	$NO + NH \rightarrow H + N_2O$	3.03×10^{-17}	0.0		[41]
(216)	$NO + H + N_2 \rightarrow HNO + N_2$	1.57×10^{-44}	0.0		[41]
(217)	$NO_2 + N \rightarrow N_2O + O$	3.0×10^{-18}	0.0		[37]
(218)	$NO_2 + O \rightarrow NO + O_2$	1.0×10^{-17}	0.0		[37]
(219)	$NO_2 + NH_2 \rightarrow H_2O + N_2O$	3.27×10^{-18}	0.0		[41]
(220)	$OH + N \rightarrow NO + H$	4.2×10^{-17}	0.0	S1, S2	[43]
(221)	$OH + NH_3 \rightarrow H_2O + NH_2$	3.32×10^{-17}	0.0	S1, S2	[43]
(222)	$OH + NH_2 \rightarrow H_2O + NH$	3.32×10^{-17}	0.0		[43]
(223)	$OH + NH \rightarrow H + HNO$	3.0×10^{-18}	0.0		[43]
(224)	$OH + N_2H \rightarrow N_2 + H_2O$	5.0×10^{-17}	0.0		[32]
(225)	$OH + OH \rightarrow H_2O_2$	$1.5 \times 10^{-17}(T_g/300)^{-0.37}$	0.0		[30]
(226)	$HNO + NH_2 \rightarrow NH_3 + NO$	5.36×10^{-18}	0.0		[36]
(227)	$HNO + H \rightarrow H_2 + NO$	3.0×10^{-17}	0.0		[36]
(228)	$HNO + OH \rightarrow H_2O + NO$	2.4×10^{-18}	0.0		[43]
(229)	$N_2(B\,^3\Pi_g) \rightarrow N_2(A\,^3\Sigma_u^+) + h\nu$ 1045 nm	$1.5 \times 10^5\ s^{-1}$	0.0		[20]
(230)	$N_2(C\,^3\Pi_u) \rightarrow N_2(B\,^3\Pi_g) + h\nu$ 337.1 nm	$2.7 \times 10^7\ s^{-1}$	0.0	S1, S2	[20]
(231)	$N_2(a'\,^1\Sigma_u^-) \rightarrow N_2 + h\nu$ 177 nm	$1.0 \times 10^2\ s^{-1}$	0.0		[44]
(232)	$N_2(A\,^3\Sigma_u^+) \rightarrow N_2 + h\nu$ 293 nm	$5.0 \times 10^{-1}\ s^{-1}$	0.0		[44]
(233)	$NO(A\,^2\Sigma^+) \rightarrow NO + h\nu$ 236.3 nm	$5.0 \times 10^6\ s^{-1}$	0.0	S1, S2	[39]
(234)	$NO(B\,^2\Pi) \rightarrow NO + h\nu$ 316 nm	$5.0 \times 10^5\ s^{-1}$	0.0	S1, S2	[45]
(235)	$O(^1S)N_2 \rightarrow O(^1D) + N_2 + h\nu$ 557.7 nm	$1.0 \times 10^7\ s^{-1}$	0.0	S2	[39]

[a] Rate coefficients have units of $m^3\ s^{-1}$ for two-body reactions and $m^6\ s^{-1}$ for three-body reactions; T_e has units eV; T_g has units K.
[b] BOLSIG$^+$ can be found in [8].
[c] S1: Simplified Chemistry 1; S2: Simplified Chemistry 2.

de-excitation into an excited, metastable or ground state; and light emission from an excited or metastable state. The light emissions of excited species of nitrogen and nitrogen oxide, and electronegative ions are all considered in the model. For NO-γ emission bands, direct electron impact excitation (e + NO $\rightarrow$ NO(A) + e) is negligible compared with the $N_2(A)$ quenching channel ($N_2(A)$ + NO $\rightarrow$ N_2 + NO(A)) [13].

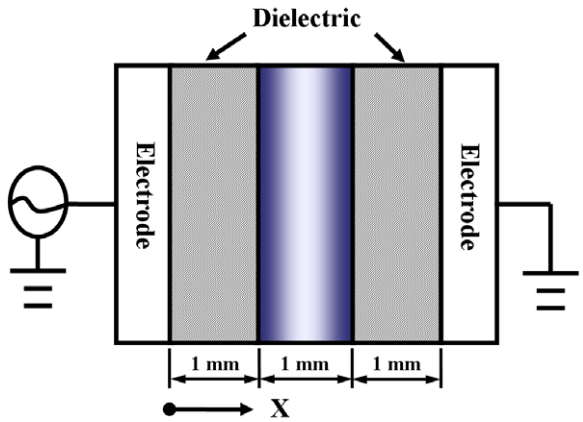

Figure 1. Schematic diagram of the 1D AP-DBD used in this study.

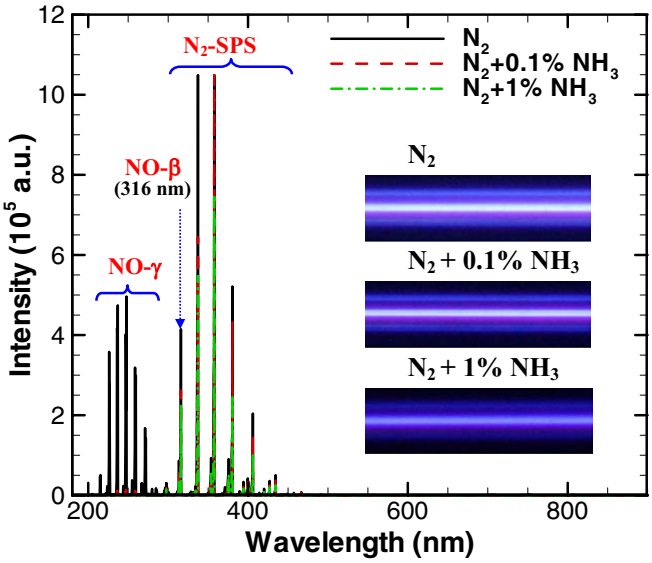

Figure 2. Optical emission spectra of the N_2/(0–1%)NH_3 AP-DBD from 180 to 900 nm under experimental conditions (30 kHz, 8 kV, 50 SLM, 400 W).

3. Results and discussion

3.1. Optical emission spectral measurements

Figure 1 shows a schematic diagram of the $N_2/O_2/NH_3$ AP-DBD. The discharge occurred within a 1 mm gap between two electrodes that were each covered with a quartz plate ($5 \times 5\,cm^2$) having a measured relative permittivity of 4.76 (quartz) and a thickness of 1 mm. The powered electrode (left) was driven by an ac power source (30 kHz) with highly distorted sinusoidal voltages, and the right electrode was grounded throughout the cycle. Additional details can be found in Chiang *et al* [14]. We performed the experiments with addition of 0%, 0.01%, 0.1%, 0.5% and 1.0% ammonia.

Figure 2 shows the optical emission spectra of the OES measurements for the wavelength range 180–900 nm in the discharge region under different concentrations of ammonia addition, ranging from 0% to 1%. Corresponding photos of visualization of fluorescence generated by the discharge between two electrodes are also included in figure 2. In the OES measurements, the emission bands of the N_2 second positive system (SPS) (313.6–466.7 nm), NO-γ (220–280 nm) and NO-β (280–380 nm) were detected. Detection of optical emissions containing O, such as NO-γ and NO-β, in a mixture of pure N_2 and NH_3 is unlikely. The presence of NO-γ and NO-β emissions in the experiments should be attributed to the impurities in commercial bottles of nitrogen (99.99% in Taiwan), such as O_2 (~30 ppm), which was carefully verified by gas chromatography prior to the discharge measurements in our laboratory. The results show that the intensities of NO-γ, NO-β and N_2-SPS decrease with increasing amount of NH_3. Furthermore, the emission of NO-γ diminishes rapidly and vanishes afterwards upon reaching an NH_3 concentration of 0.5%. In contrast, the other two emission lines decrease only slightly with increasing NH_3 levels. The decreasing intensities of these emission lines due to the addition of ammonia were predicted using the self-consistent fluid model, which are presented next.

3.2. Simulation conditions

In the fluid model, a background gas temperature of 400 K and an impurity oxygen level of 30 ppm were assumed. After careful grid convergence testing, 210 computational cells with non-uniform spacing provided sufficient accuracy throughout the study. The 210 computational cells include a dielectric mesh (10 cells) and a plasma mesh (200 cells). The mesh in the dielectric layer is uniform with 0.2 mm in size per cell. The grid convergence criterion is based on the fact that essentially no changes (<1%) of cycle-averaged number densities of several important species are found when the grid is refined. The sizes of the smallest and largest cells in the mesh of the plasma region are 1.58 μm near the wall and 11.52 μm in the bulk, respectively. The time step is set to 10^{-10}–10^{-11} s, unless otherwise specified. This is kept as a constant for the condition of fixed ammonia concentration, while it decreases with increasing ammonia concentration. The electrical properties and distributions of all of the charged species of the discharge remained mostly unchanged after 3–5 simulation cycles, although the neutral species were still evolving slightly. Here, we present the results obtained with the 20th cycle. The resulting total number of time steps for 0% and 1% NH_3 are 6.6 and 66 million time steps, respectively.

3.3. Validation with the experimental results

To demonstrate the accuracy of the 1D self-consistent fluid model for the N_2/NH_3 AP-DBD considering oxygen impurity that predicts the light emissions from NO-γ, NO-β and N_2-SPS, we first compared the simulations with earlier experimental data obtained under similar conditions without addition of NH_3 [15]. Figure 3 shows the simulated spatio-temporal density distributions of $N_2(C)$ and $N_2(A)$ along with the applied voltages (black solid line) and conduction currents (red dashed line) in a cycle with a gas mixture of 300 ppm O_2 in N_2 and an estimated oxygen impurity level of 15 ppm under Brandenburg's experimental conditions [15]. These conditions corresponded to a frequency of 6.94 kHz, a sinusoidal voltage of amplitude of 9.7 kV, a gap of 1.1 mm, dielectric barriers with thicknesses of 2.05 and 2.3 mm and a

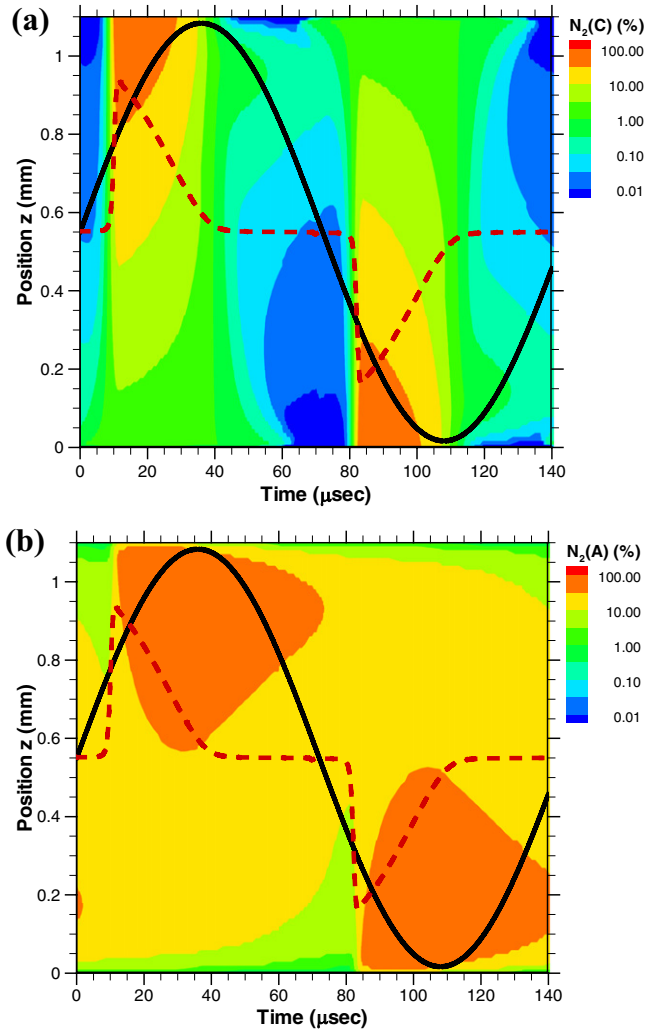

Figure 3. Spatio-temporal distributions of (a) $N_2(C)$ and (b) $N_2(A)$ under the same experimental conditions as those of Brandenburg [15].

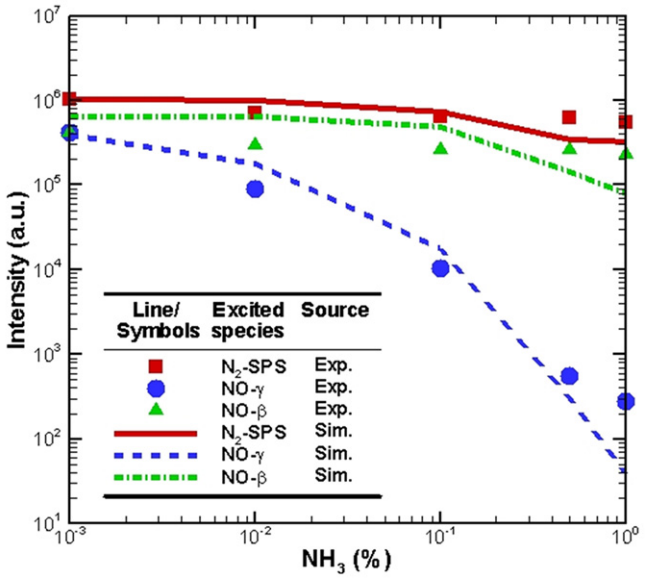

Figure 4. Optical emission spectra comparison of simulations with experiments. (Note that 0.001% NH_3 really represents 0% NH_3 on the x-axis.)

permittivity of 4.6, a pressure of 1 atm and a gas temperature of 300 K. The simulated spatio-temporal density distributions of $N_2(C)$ and $N_2(A)$ agree reasonably well with the measured spatio-temporal intensity distributions of N_2-SPS and NO-γ [15], although there is a time delay ($\sim$15 μs) between the simulated and measured major breakdowns for the maximal level of contour. The density distributions of $N_2(C)$ and $N_2(A)$ can be compared directly with the measured intensity distributions because the effective lifetimes of $N_2(C)$ and NO(A) are much shorter than the timescale of the density evolution and also because NO(A) is mainly generated by reaction (R111) ($N_2(A)$+NO$\rightarrow N_2$+NO(A)) [15].

Figure 4 shows the comparison between the predicted and measured light intensities in the discharge. The simulated light intensity of N_2-SPS was adjusted to match the measurements without ammonia addition. For a better visual arrangement of the data, we have shifted both data points to 0.001% of ammonia addition. We then scaled all of the simulated light intensities, including N_2-SPS, NO-γ and NO-β, proportionally. For the discussion, specific wavelengths of the emitted light were selected: 337.1 nm (N_2-SPS), 236 nm (NO-γ) and 316 nm (NO-β). The results show that all of the measured light intensities of the discharges decrease with increasing concentration of ammonia, particularly NO-γ, which decreases dramatically. All of the trends of the three major emission lines were captured by the simulations, and this indicates that the current fluid modeling is reasonably successful in reproducing the physics of the gas discharge. The spectral intensities in the discharges are dominated by N_2-SPS, which is induced by electron-impact excitation of ground-state nitrogen, whose effective lifetime is on the order of nanoseconds. Additional details about these emission lines will be explained by exploring the discharge properties and are presented next.

3.4. Distributions of the species number densities

Figure 5 shows several typical spatio-temporal averaged number densities of charged, excited and neutral species as a function of the amount of added ammonia under the same test conditions as presented in figure 4. Figure 5(a) shows that the densities of the electrons and most ionic species decrease with increasing amounts of added NH_3, except for NH_4^+ and H^-. The decrease in the electron density is caused by direct electron attachment ((R22): $e + NH_3 \rightarrow NH_2 + H^-$) [16] because NH_3 is an electronegative gas that has high electron affinity. This also induces a rapid increase in the production of negative atomic hydrogen with increasing amounts of NH_3. The electron temperature increases slightly with increasing ammonia addition from 3.6 to 3.7 eV. For added NH_3 concentrations less than 0.1%, the dominant charged species is N_4^+, which is produced by a charge-exchange reaction ((R46): $N_2^+ + N_2 + N_2 \rightarrow N_4^+ + N_2$). This process becomes less efficient as N_2^+ decreases with increasing NH_3. For NH_3 concentrations greater than 0.1%, the dominant charged species becomes NH_4^+, caused by charge exchange with NH_2^+

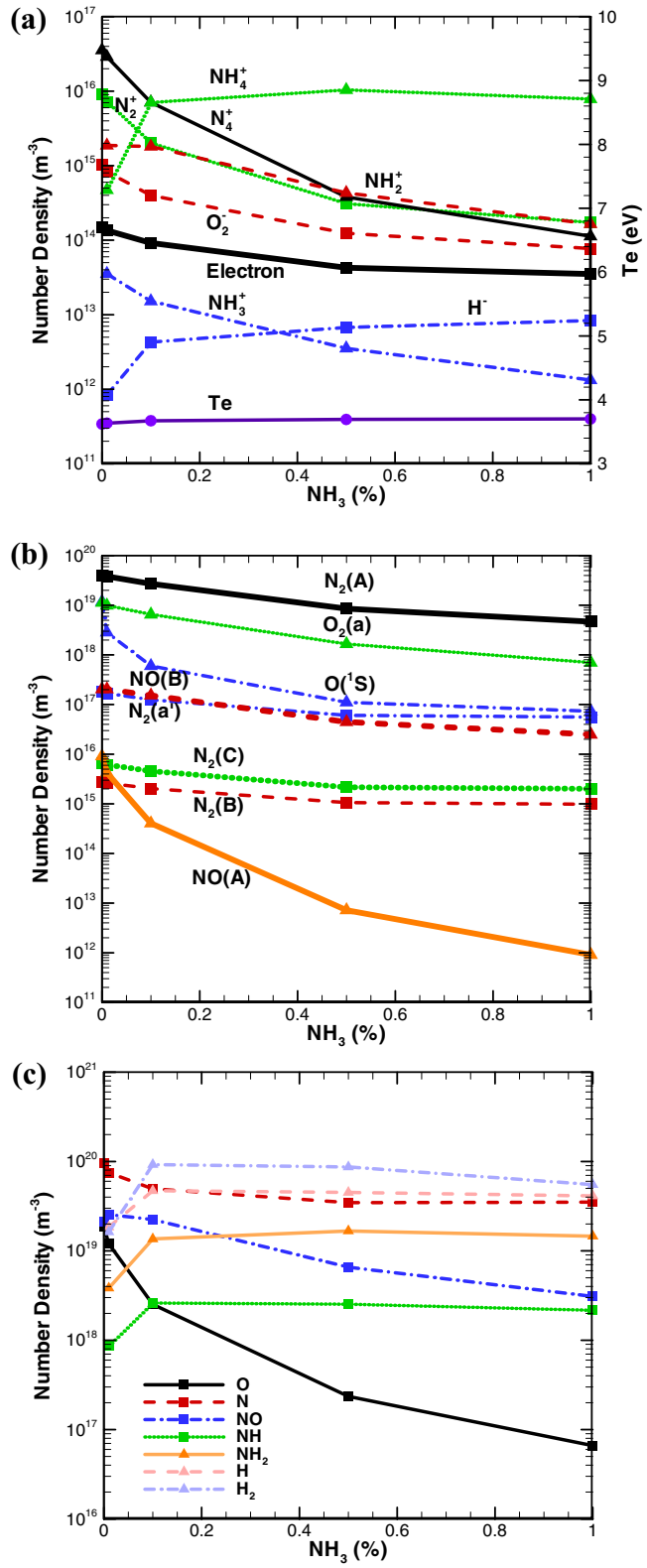

Figure 5. Spatio-temporal averaged number density of (*a*) charged, (*b*) excited and (*c*) neutral species as a function of the concentration of ammonia from 0% to 1%.

and NH_3^+ through reactions (R58) ($NH_2^+ + NH_3 \rightarrow NH_4^+ + NH$) and (R61) ($NH_3^+ + NH_3 \rightarrow NH_4^+ + NH_2$). In addition, NH_4^+ rapidly increases with increasing NH_3 initially, and it then becomes saturated with further increases in NH_3, which is caused by the rapid decrease in NH_2^+ through (R58) ($NH_2^+ + NH_3 \rightarrow NH_4^+ + NH$), which cancels out the effect by the linearly increasing ammonia. In fact, NH_3^+ and NH_2^+ are generated though reactions (R47) ($N_2^+ + NH_3 \rightarrow NH_3^+ + N_2$), (R52) ($N_4^+ + NH_3 \rightarrow NH_3^+ + 2N_2$) and (R60) ($NH_3^+ + NH_3 \rightarrow NH_2^+ + H_2 + NH_2$), in which N_2^+ and N_4^+ are exchanged with NH_3, respectively, to form NH_3^+. Therefore, N_2^+ and N_4^+ are both effectively transformed into NH_4^+ and decrease with increasing amounts of NH_3.

Figure 5(*b*) shows that the number densities of all of the excited species decrease with increasing amounts of ammonia. As expected, $N_2(A)$ remains the dominant excited species in nitrogen with oxygen impurities (without the addition of ammonia) as in a pure nitrogen DBD [17]; however, $N_2(A)$ undergoes an approximately 10-fold decrease when 1% of ammonia is added. Note that $N_2(A)$ is mainly generated by excited/neutral de-excitation of $N_2(B)$ by ground-state N_2 ((R116): $N_2(B) + N_2 \rightarrow N_2(A) + N_2$) and is removed by the metastable–metastable excitation ((R106): $N_2(A) + N_2(A) \rightarrow N_2(C) + N_2$), the metastable–neutral de-excitation ((R112): $N_2(A) + NH_3 \rightarrow N_2 + NH_2 + H$) and the metastable–neutral de-excitation dissociation ((R113): $N_2(A) + NH_3 \rightarrow N_2 + NH + H_2$). N_2-SPS is primarily produced by the de-excitation of $N_2(C)$ (R230), which is also generated by the electronic excitation of nitrogen ((R9): $e + N_2 \rightarrow N_2(C) + e$) and removed by the metastable–neutral de-excitation mechanism ((R127): $N_2(C) + N_2 \rightarrow N_2(a^{'1}) + N_2$). This leads to a slight decrease in $N_2(C)$ that is caused by the decrease in electrons due to the addition of ammonia as mentioned earlier. N_2-SPS emission is proportional to the amount of $N_2(C)$, which explains the slight decrease in N_2-SPS emission with increasing amounts of NH_3 in both simulations and experiments (figure 4). In addition, NO-γ emission is produced by de-excitation of NO(A) (R233), which is generated by the two-body collision reaction (R111) ($N_2(A) + NO \rightarrow N_2 + NO(A)$) and destroyed by reaction (R150) ($NO(A) + NH_3 \rightarrow NO + NH_3$), whose destruction rate is proportional to the amount of ammonia added. $N_2(A)$ is removed via (R106), (R112) and (R113), leading to a decrease in NO(A) through (R111). These findings explain the rapid decrease in NO-γ emission in both simulations and experiments, as presented in figure 4. Moreover, NO-β is destroyed through reaction (R234) ($NO(B) \rightarrow NO + h\upsilon$) and is created by the three-body reactions (R156) ($N + O + N_2 \rightarrow NO(B) + N_2$) and (R157) ($N + O + NH_3 \rightarrow NO(B) + NH_3$), which are two competing reactions because atomic oxygen decreases rapidly with increasing amounts of NH_3. This leads to a slight decrease in NO-β emission with increasing amounts of NH_3 (figure 4).

Figure 5(*c*) shows the number densities of the neutral species as a function of the amount of added NH_3. One immediate observation is that the amount of all of the neutral species containing H atoms increases rapidly up to 0.1% upon addition of NH_3 and levels off afterwards. As mentioned earlier, the concentrations of N, O and NO, affecting the generation and removal of NO-γ and NO-β, decrease with increasing amounts of NH_3. For concentrations of NH_3 less than 0.1%, atomic nitrogen is the dominant neutral product, which is generated through the electron-impact dissociation of

N_2 ((R10): e + N_2 → N + N + e) and removed through the following reactions: (R156) (N + O + N_2 → NO(B) + N_2), (R157) (N + O + NH_3 → NO(B) + NH_3), (R183) (N + NH_2 → 2H + N_2) and (R211) (NO + N → N_2 + O). For concentrations of NH_3 greater than 0.1%, the dominant neutral speices becomes H_2 generated by reactions (R60) and (R113). The results mean that a small amount of added ammonia into a nitrogen (with oxygen impurities) AP-DBD can be used to produce abundant hydrogen. Similar results were also observed in a numerical study on H_2 generation in an Ar/NH_3 microdischarge [18]. The amount of atomic nitrogen decreases with increasing amounts of NH_3 and becomes saturated as more ammonia is added. The decreasing trend of N with increasing ammonia is due to the reduction in electron density following attachment reactions with ammonia, as shown in (R22) (e + NH_3 → NH_2 + H^-).

In addition, the number density of atomic oxygen is decreased by approximately two to three orders of magnitude with an increase in NH_3 concentration from 0% to 1%, mainly through the destructive reactions (R108) ($N_2(A)$ + O → O(^{1}S) + N_2), (R156) (N + O + N_2 → NO(B) + N_2) and (R157) (N + O + NH_3 → NO(B) + NH_3). This may explain the recent experimental results of Yang *et al* [2] showing that the measured surface roughnesses of PLA surfaces treated with N_2/5% NH_3 and N_2/0.1% O_2 AP-DBDs with an oxygen impurity level of 30 ppm in nitrogen are 1.5 nm and 50.16 nm, respectively. This indicates that the discharge of N_2/0.1% O_2 has a higher etch rate because the etch rate is proportional to the amount of atomic oxygen [19]. Moreover, NO is generated by reactions (R150) (NO(A) + NH_3 → NO + NH_3), (R233) (NO(A) → NO + $h\upsilon$) and (R234) (NO(B) → NO + $h\upsilon$), and lost by reactions (R111) ($N_2(A)$ + NO → NO(A) + N_2), (R211) (NO + N → N_2 + O) and (R213) (NO + NH_2 → N_2 + H_2O). The densities of NH and NH_2 are approximately constant with NH_3 addition in the range 0.1–1%.

3.5. Discharge structure in the N_2/O_2 and $N_2/O_2/NH_3$ discharges

Figure 6 shows snapshots of the spatial distributions of various plasma properties of the N_2/O_2 and N_2/O_2/1% NH_3 discharges at the maximum current density, in which oxygen with an oxygen impurity level of 30 ppm is considered. The results show that the number density of electrons grows rapidly from the cathode to the anode, ions outnumber electrons, except at the anode, and the electric field increases slightly from the anode to the cathode for both discharges. These are typical features of a Townsend-like discharge [4, 13, 20, 21]. The features show that N_2^+ and N_4^+ are the two most dominant ionic species during the breakdown period in the N_2/O_2 discharge, while NH_4^+ becomes the most dominant ion through the mechanisms as explained in figure 5(a). The amount of N_2^+ is slightly more than that of N_4^+, especially near the cathode in both cases, at the instant when the current density is maximal. In addition, the electric field across the gap becomes weaker as 1% of NH_3 is added into the N_2/O_2 discharge. Figure 6(c) shows that most surface charge is caused mainly by the highly mobile electrons on the powered dielectric and by N_2^+ and NH_4^+ on the grounded dielectric. N_2^+ is the most dominant surface

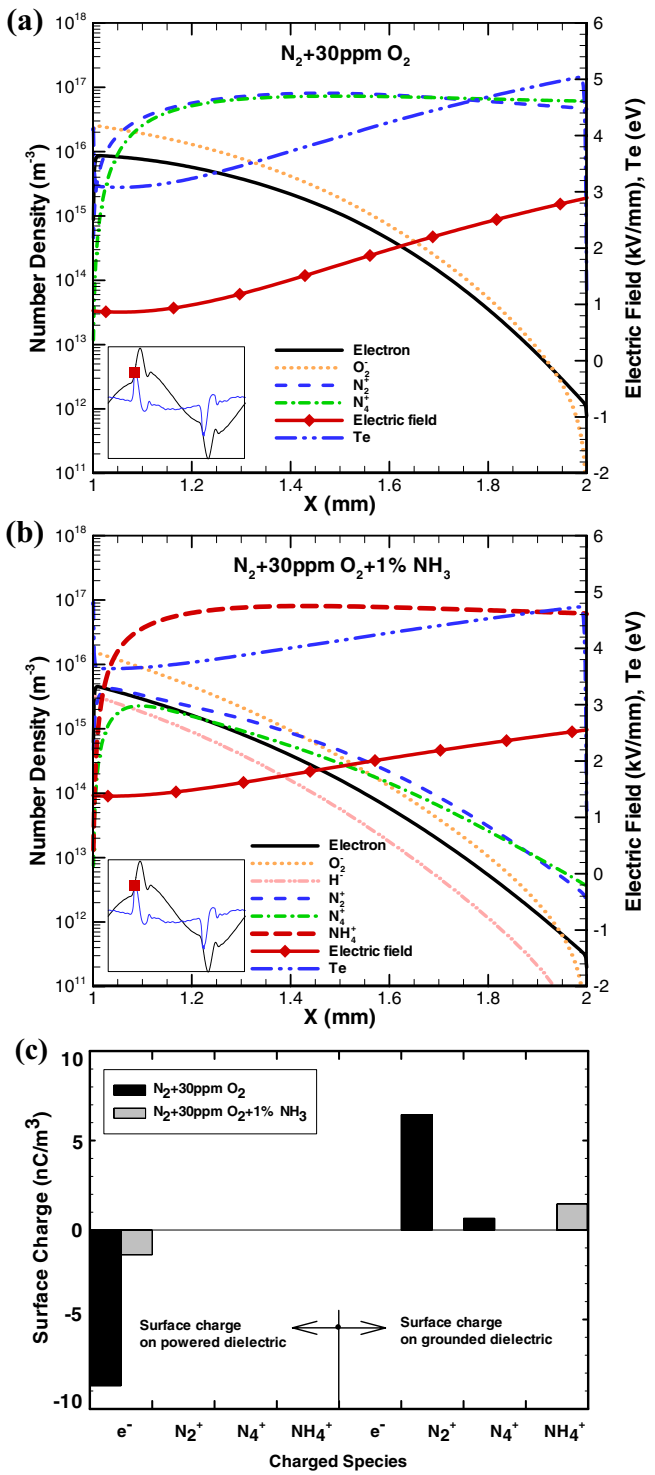

Figure 6. Snapshots of distribution of plasma properties of charged species in (a) N_2/30 ppm-O_2 and (b) N_2/30 ppm-O_2/1% NH_3 discharges, and (c) the surface charge density on dielectric comparison of N_2/30 ppm-O_2 and N_2/30 ppm-O_2/1% NH_3 at the maximum current density (the time relative to the beginning of the breakdown is 1.11 μs).

charge species on the grounded electrode side in the N_2/O_2 AP-DBD, while NH_4^+ becomes the dominant incoming charged species at the dielectric surface of the grounded electrode side in the N_2/O_2/1% NH_3 AP-DBD. It shows that the surface charges caused by the incoming electrons (powered dielectric)

and positive ions (grounded electrode) are roughly the same for both cases. However, an appreciable portion of electrons is lost in the bulk region since the amount of O_2^- (through electron attachment) is even more than that of electrons in the case of N_2/O_2 AP-DBD. The situation becomes even more obvious in the case of $N_2/O_2/1\%$ NH_3 AP-DBD since H^- is also non-negligible because of electron attachment in addition to the appreciable amount of O_2^- (figure 6(*b*)).

Figure 7(*a*) shows the temporal distributions of the spatially averaged number densities of electron, O_2^-, N_2^+ and N_4^+. The amount of N_2^+ approaches that of N_4^+ during the breakdown period (~6 μs) because the direct ionization of nitrogen by electron impact becomes a dominant channel for ionization. As shown in figures 6(*b*) and 7(*b*), NH_4^+ becomes the most dominant ionic species in the $N_2/O_2/1\%$ NH_3 AP-DBD because N_2^+ and N_4^+ are exchanged with NH_3 to form NH_4^+ indirectly and effectively, as described in section 3.3. In previous experimental studies, the homogeneous discharges of nitrogen with oxygen impurities (less than 400 ppm [15, 22, 23] also showed typical Townsend-like discharges. The numerical results for the N_2/O_2 discharge are also consistent with several similar experimental observations [13, 15, 23]. Figure 7(*c*) shows that, at the beginning of the breakdown, most surface charge is caused mainly by the highly mobile electrons on the powered dielectric, and N_2^+ (N_2/O_2 AP-DBD case) and NH_4^+ ($N_2/O_2/1\%$ NH_3 AP-DBD case) on the grounded dielectric and, during the peak of the breakdown, the surface charge at the powered electrode reaches a very high value also by the electrons. In the second breakdown of the cycle (negative powered electrode), N_2^+ gradually becomes the most dominant surface discharge species at the powered dielectric. As ammonia is added, the electrons attached to the dielectric surface of the positive powered dielectric becomes much fewer, although still dominant in the early part of the cycle. Interestingly, in the second breakdown of the cycle, NH_4^+ becomes the dominant charged species at the negative powered dielectric, although the amount becomes much smaller as compared with that without the addition of ammonia. A comparison of figures 7(*a*) and (*b*) shows that the spatially averaged electron temperature for the N_2/O_2 discharge is slightly less than that for the $N_2/O_2/1\%$ NH_3 discharge.

Figure 8 shows the spatio-temporal distributions of electron temperature with the temporal discharge current density in a cycle (curves in black) for the N_2/O_2 and $N_2/O_2/1\%$ NH_3 discharges. The results show that the period (6–7 μs), when the highest electron temperature appears close to the cathode in the N_2/O_2 DBD, is longer temporally and wider spatially as compared with that of the $N_2/O_2/1\%$ NH_3 DBD during the breakdown period, even though the spatially averaged electron temperature is lower in the N_2/O_2 DBD.

Figure 9 shows the spatio-temporal distributions of N_2-SPS light emission with the temporal current density in a cycle for the N_2/O_2 and $N_2/O_2/1\%$ NH_3 discharges. The light emission intensity (W m^{-3}) is computed as $A \times N \times h \times (c/\lambda)$, where A is the Einstein coefficient (s^{-1}), N is the number density of excited species (m^{-3}), h is the Planck constant (J s), c is the speed of light (m s^{-1}) and λ is the wavelength (m). The period (~6–7 μs) with the highest intensity in the

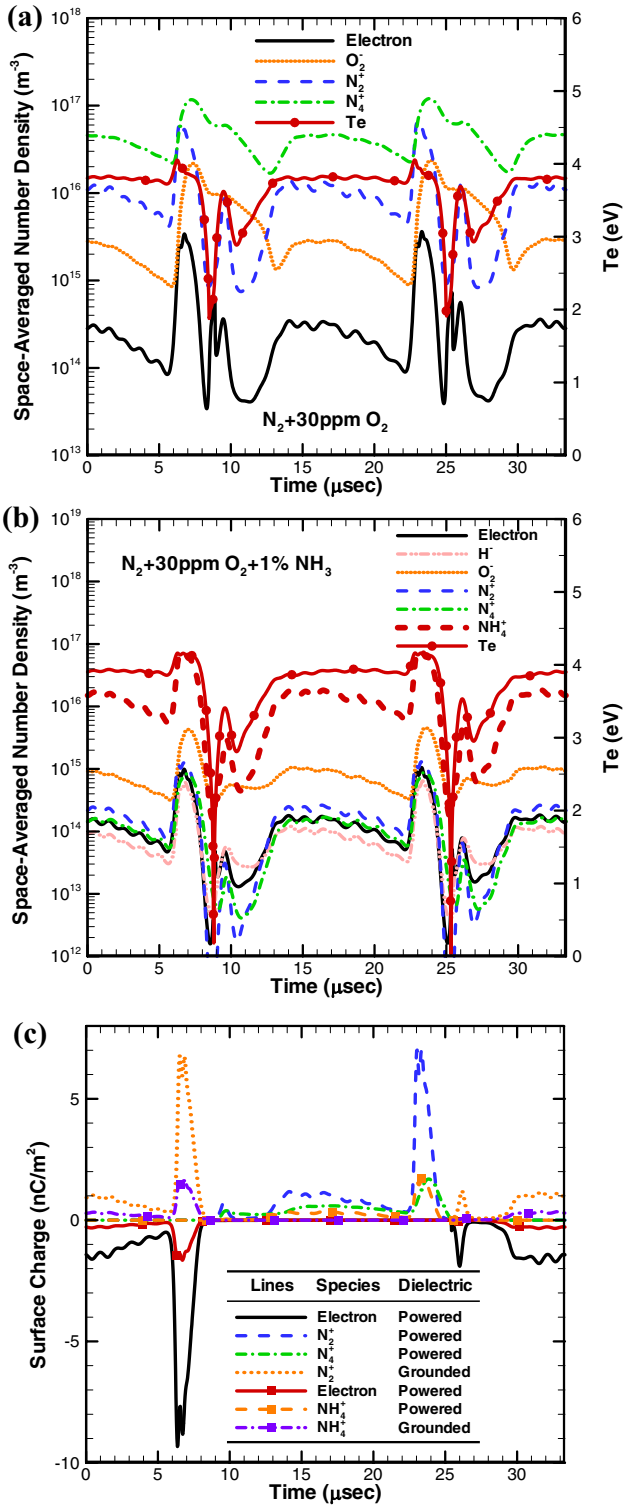

Figure 7. Temporal profiles of space-averaged number densities of charged species in (*a*) N_2/30 ppm-O_2 and (*b*) N_2/30 ppm-O_2/1% NH_3 discharges in a cycle, and (*c*) the comparison of temporal profiles of surface charge density on the dielectric between N_2/30 ppm-O_2 (pure curves) and N_2/30 ppm-O_2/1% NH_3 (curves with symbols) discharges in a cycle.

spatial distribution of the N_2-SPS light emission in the N_2/O_2 DBD becomes narrower temporally and elongated spatially compared with that of the $N_2/O_2/1\%$ NH_3 DBD during the breakdown period. In addition, the results showing the

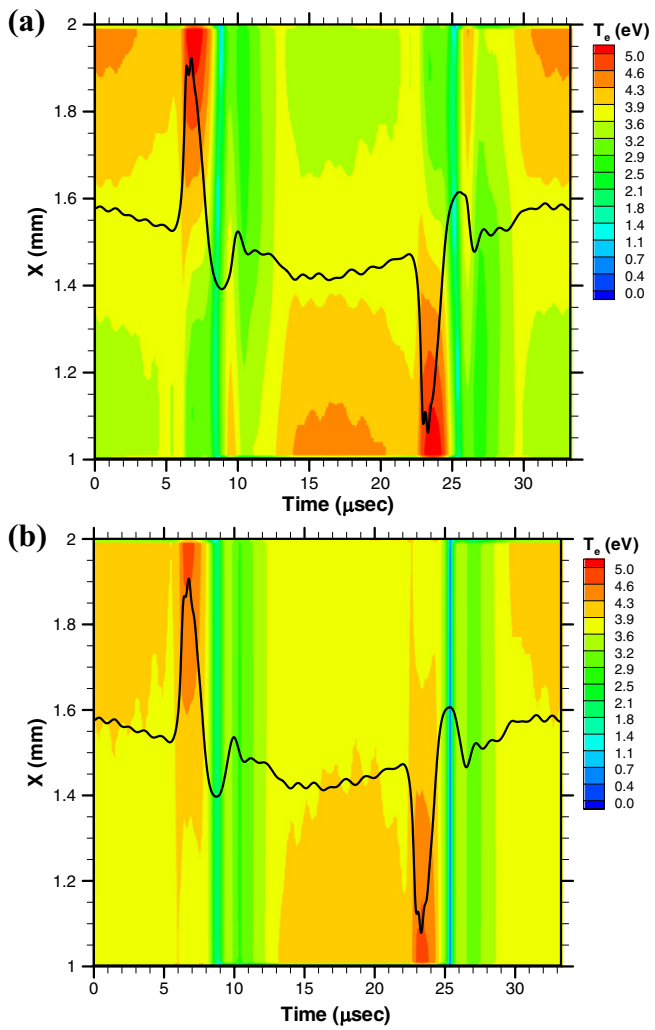

Figure 8. Spatio-temporal distribution of electron temperature in (*a*) N_2/30 ppm-O_2 and (*b*) N_2/30 ppm-O_2/1% NH_3 in a cycle.

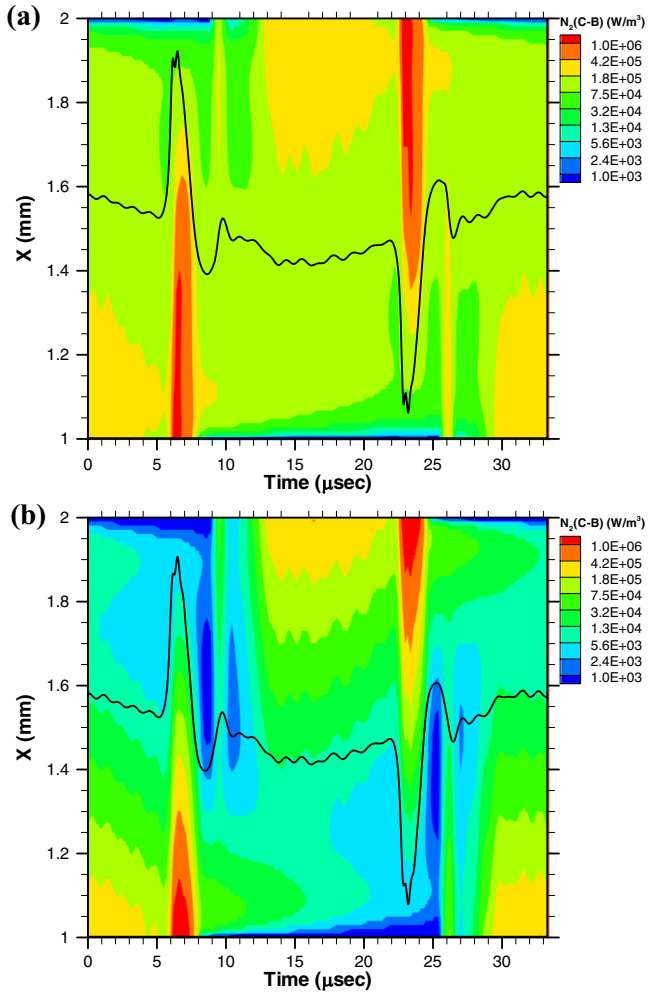

Figure 9. Spatio-temporal distribution of light emission intensity of N_2-SPS in (*a*) N_2/30 ppm-O_2 and (*b*) N_2/30 ppm-O_2/1% NH_3 discharges in a cycle.

maximal light emission near the anode are characteristics of Townsend-like discharges [13, 15, 21]. Thus, all of the results indicate that the discharges are typical Townsend-like discharges even for discharges with ammonia added into nitrogen with oxygen impurity.

3.6. Power absorption in the N_2/O_2 and $N_2/O_2/NH_3$ discharges

To understand the change in the discharge structure of a nitrogen/oxygen DBD due to the addition of ammonia, we investigated the related power absorptions in the following. Instantaneous power absorption is calculated by the integration of the current density multiplied by the electric field over the entire discharge space. Figure 10(*a*) shows the temporal distributions of power absorption of the charged species and the displacement current in the N_2/O_2 DBD in a cycle. The results show that the dominant species for power absorption are electrons and N_2^+ during the gas breakdown. In figure 7(*a*), N_2^+ and N_4^+ are the dominant ions with similar levels during the breakdown period in the N_2/O_2 DBD. This is in contrast to the case for the pure N_2 DBD in which N_4^+ is the dominant charged species [17]. Because N_2^+ is much lighter than N_4^+ (thus, higher mobility), the former absorbs more power than the latter.

Figure 10(*b*) shows the temporal distributions of the power absorbed by the charged species and the displacement current in a cycle when 1% NH_3 is added into the N_2/O_2 DBD. The results show that the dominant species for power absorption becomes NH_4^+ in both gas breakdowns in a cycle, rather than electrons or N_2^+. The major cause is that a large amount of NH_4^+ is generated through reactions (R58) ($NH_2^+ + NH_3 \rightarrow NH_4^+ + NH$) and (R61) ($NH_3^+ + NH_3 \rightarrow NH_4^+ + NH_2$) during the gas breakdowns, while the production of N_2^+ and N_4^+ is strongly suppressed because N_2^+ and N_4^+ charge exchange with NH_3 to form NH_3^+ via reactions (R47) and (R52), respectively. In addition, because NH_4^+ is lighter than N_2^+ and N_4^+, by comparing figures 10(*a*) and (*b*), we found that the power absorbed by the ionic species (NH_4^+) increases appreciably (~30%) as 1% NH_3 is added into the N_2/O_2 DBD. At the same time, the power absorbed by the electrons decreases significantly (~40%) due to the reduced electron number density with increasing NH_3 concentration. In brief, no matter whether ammonia is added or not, the power absorbed by the ionic charged species in the N_2/O_2 DBD is much higher than that by the electrons.

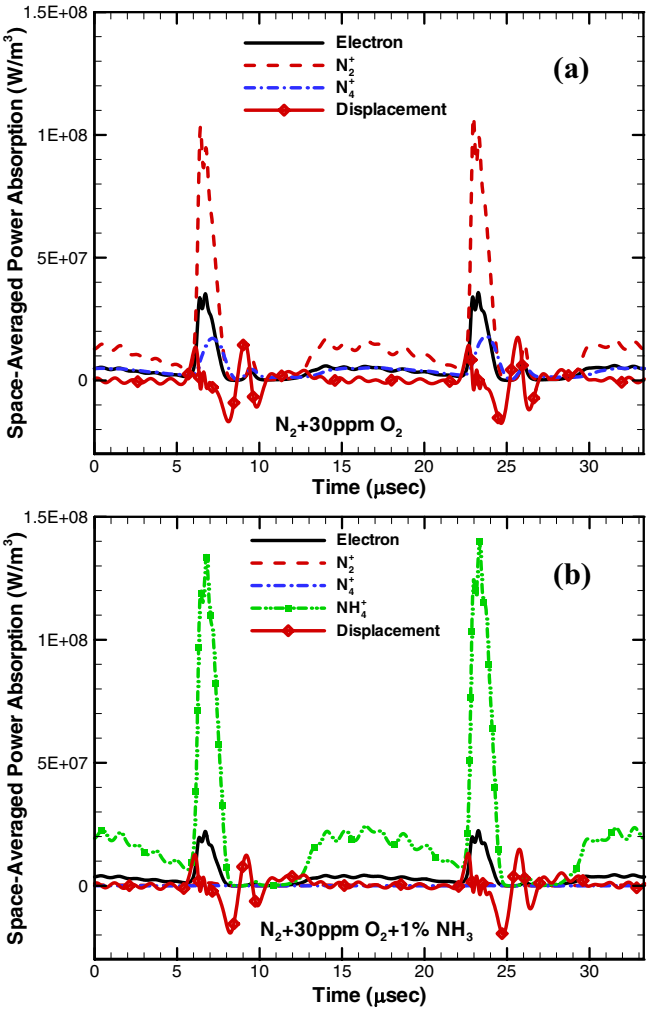

Figure 10. Temporal power absorption in (*a*) N_2/30 ppm-O_2 and (*b*) N_2/30 ppm-O_2/1% NH_3 discharges.

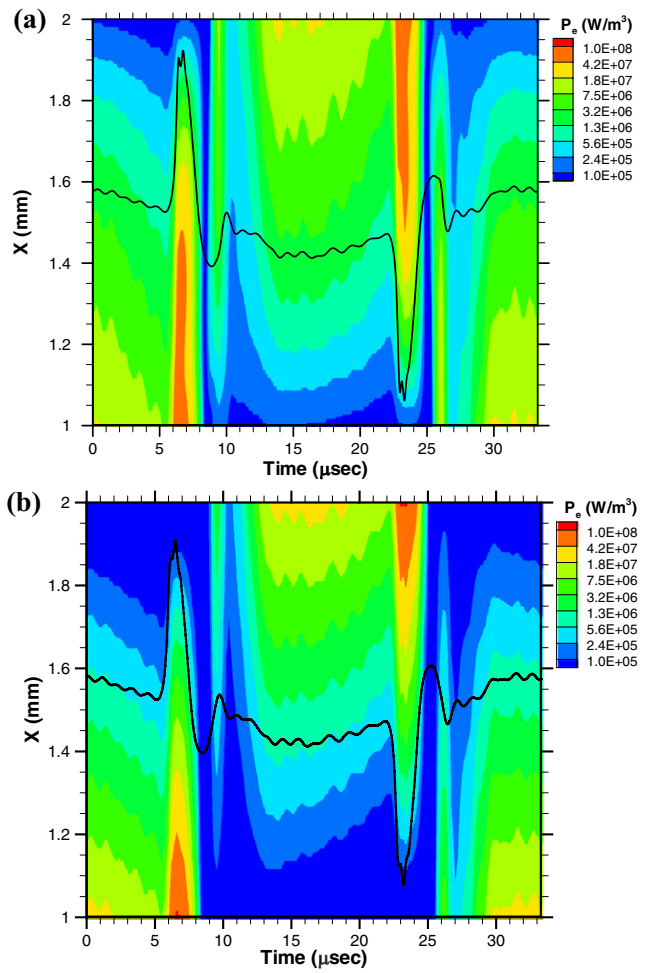

Figure 11. Spatio-temporal distribution of electron power absorption in (*a*) N_2/30 ppm-O_2 and (*b*) N_2/30 ppm-O_2/1% NH_3 in a cycle.

Figure 11 shows the spatio-temporal distributions of the power absorbed by the electrons along with the simulated temporal current densities (curves in black) in the N_2/O_2 and N_2/O_2/1% NH_3 DBDs. The results show that the power absorbed by the electrons decreases with increasing NH_3 because the number of electrons decreases with increasing NH_3. This finding reveals that the light emission weakens with increasing NH_3 because there are fewer electrons that can excite the molecules. Most importantly, the trend of the simulated light intensities agrees with the experimental results shown in figure 2.

3.7. Algorithm for reducing chemical kinetics

For efficient multidimensional fluid modeling, one often needs to reduce the original complex plasma chemistry to an acceptable set of chemical reactions, which can significantly reduce the runtime without sacrificing the accuracy. In a typical non-plasma reactive system, a global model (0D), which calculates both sensitivity coefficients and rates of production (ROPs) of all reactions to any species efficiently, is generally employed to reduce the chemical kinetics mainly because of its minimal computational cost needed. However, in a reactive plasma system, no effect of both frequency and voltage waveform of a power source and the electric field can be correctly investigated in a global model alone, even though they play important roles in discharge properties. Thus, a combination of both the 0D global model and the 1D fluid model becomes necessary to reduce the complex plasma chemistry properly and accurately.

Figure 12 shows a flowchart of how to deduce the reduced chemical kinetics from a set of more complete plasma chemistry by combining the global model with the 1D fluid model. In the first step, the global model (0D) using the original complex chemical kinetics is performed via the Plasma PSR module of Chemkin version 4.1.1 [6] using the simulated results with the original complex plasma chemistry from the 1D fluid modeling as the initial conditions.

In the second step, we construct a tentative reduced chemical kinetics based on the analysis of the ROPs and sensitivity coefficients from the 0D Chemkin simulation. The basic principle of chemical kinetics reduction is to select those species and reactions based on the criterion for those reactions which have ROP larger than some criterion (e.g. 1% in the current study) corresponding to the selected species, and also to include the reaction with the dominant sensitivity coefficient

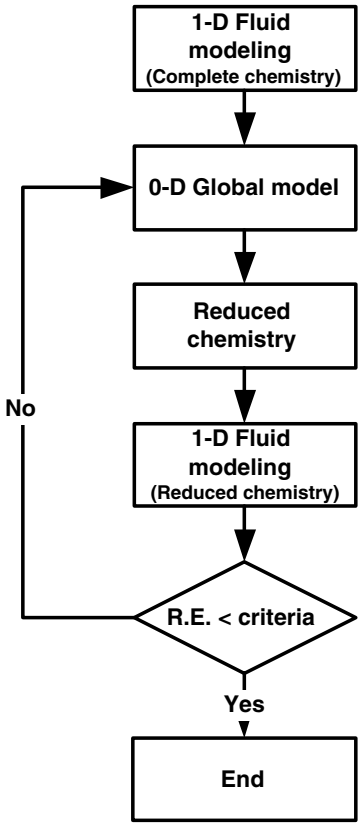

Figure 12. Flowchart of reduced chemistry.

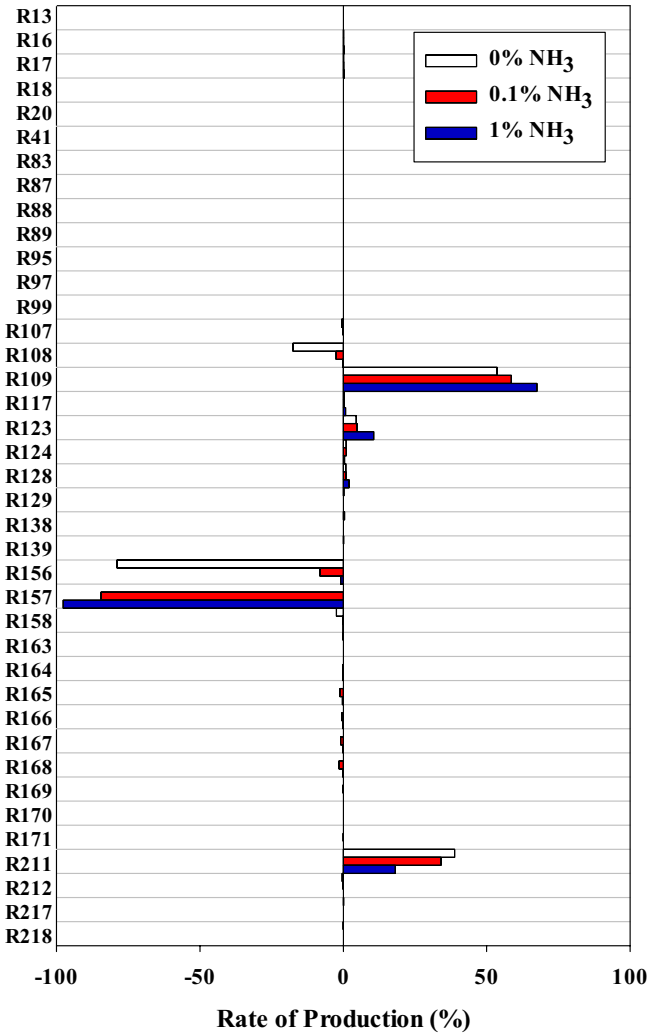

Figure 13. Comparison of ROP of atomic oxygen among various levels of ammonia addition in a N_2/O_2 discharge.

to the selected species even if its ROP is lower than the criterion. We then select those species with neutral densities more than 10^{-18} m^{-3} in the case of $N_2/O_2/NH_3$ discharge based on the 1D fluid modeling. All the reactions that produce and consume the unselected species are removed from the reduced set of plasma chemistry. The sensitivity analysis [24, 25] is employed to determine the influential reactions that are the most relevant to the interested species as described above. In general, the sensitivity analysis provides complementary information to the ROP analysis. The ROP analysis is employed to determine the major reactions that produce and consume the selected species. ROP can be calculated as

$$\mathrm{ROP}_{i,k} = \frac{R_{i,k}}{\sum_{j=1}^{m} R_{j,k}} \times 100\% \qquad (1)$$

where $R_{i,k} = k_i N_A N_B$ denotes the reaction rate of the ith reaction channel related to the kth selected species, which has units m^{-3} s^{-1}; k_i denotes the rate constant; N_A and N_B denote the densities of reactants A and B in the ith reaction channel related to the kth selected species; and m denotes the total number of reaction channels related to the kth selected species. A practical example is presented next to demonstrate the process of reduction.

Figure 13 shows an example of the ROPs of the reaction channels related to atomic oxygen for different ammonia concentrations in a N_2/O_2 discharge. We select those reactions related to O with the magnitude of ROP larger than 1%, which include (R108), (R109), (R123), (R128), (R156) (R157), (R158) and (R211). In addition, one needs to re-include an unselected species in a reaction channel, if its exclusion induces a substantial error of the density of the other selected species. For example, OH (whose density is less than 10^{-18} m^{-3}) is not considered in the preliminary list of selected species, which leads to a relative error of H_2O of more than 20% because the reactions (R221): $OH + NH_3 \rightarrow H_2O + NH_2$ and (R137): $O(^1S) + H_2O \rightarrow 2OH$ are both dominant reactions for the production and loss of H_2O. Thus, OH should be considered and added to the list of selected species to reduce the error for the prediction of H_2O concentration. In addition, based on the sensitivity analysis, for example, reaction (R10) is found to be a sensitive reaction to the NO(A) species since it has the largest sensitivity coefficient. This leads to the re-inclusion of reaction (R10) in the reduced list of reactions.

In the third step, plasma simulation using the results of the simplified plasma chemistry reduced by Chemkin is carried out using the 1D fluid modeling. The results of the concentrations of the selected species are then compared with those obtained by the more complete plasma chemistry. The relative differences of species densities between the more complete and reduced 1D fluid models should be smaller than

Table 2. Summary of plasma species with various reduced chemical kinetics.

Species[a]	Chemistry[b]	Species[a]	Chemistry[b]	Species[a]	Chemistry[b]
e	S1, S2	$N(^2P)$		N_2	S1, S2
O^-		$N_2(A\,^3\Sigma_u^+)$	S1, S2	NO	S1, S2
O_2^-	S1, S2	$N_2(B\,^3\Pi_g)$	S1, S2	NO_2	
H^-	S1, S2	$N_2(a'\,^1\Sigma_u^-)$	S1, S2	N_2O	
O_2^+		$N_2(C\,^3\Pi_u)$	S1, S2	NH	S1, S2
N^+		NO(A)	S1, S2	NH_2	S1, S2
N_2^+	S1, S2	NO(B)	S1, S2	NH_3	S1, S2
N_4^+	S1, S2	$O(^1S)$	S1, S2	N_2H	S1, S2
NH^+		$O(^1D)$	S2	N_2H_2	S1, S2
NH_2^+		O_2(a)	S1, S2	N_2H_3	S1, S2
NH_3^+	S1, S2	$O(^1S)N_2$	S2	N_2H_4	
NH_4^+	S1, S2	O	S1, S2	H	S1, S2
H^+		O_2	S1, S2	H_2	S1, S2
H_2^+		O_3	S1, S2	HNO	
H_3^+		OH	S1, S2	H_2O	S1, S2
$N(^2D)$		N	S1, S2	H_2O_2	

[a] All species are included in the complete chemistry.
[b] S1: Simplified Chemistry 1; S2: Simplified Chemistry 2.

Table 3. Accuracy and computational time with various chemical kinetics.

	Complete Chemistry	Simplified Chemistry 1	Simplified Chemistry 2
Species	48	31	33
Reactions	235	80	87
Hours/cycle	8.56	3.45	4.04
Error criteria		20%	5%
Max. relative error (%) (charged + metastables)	0	4.7%	4.6%
Max. relative error (%) (all selected species)	0	19.9%	4.6%
RMSE (%)	0	4.2%	1.8%

the preset error criterion. Otherwise, the above procedure, starting from the second step but with a smaller selection criterion of species density, should be repeated until the reduced chemistry set is converged.

3.8. Proposed reduced chemical kinetics for the $N_2/O_2/NH_3$ discharge

For $N_2/O_2/NH_3$ mixtures, we have obtained two sets of simplified plasma chemistry consisting of 31 species and 80 reactions as the Simplified Chemistry 1 (S1) and 33 species and 87 reactions as the Simplified Chemistry 2 (S2). Table 2 summarizes the comparison of the selected species in the two sets of simplified chemistry. Table 3 summarizes the comparison of the accuracy and computational time using the 1D fluid modeling with various levels of chemical kinetics. The overall accuracy of the number densities of the selected species is quantified by the root mean squared error (RMSE) as

$$\mathrm{RMSE} = \sqrt{\frac{1}{N}\sum_{i=1}^{N}\left(\frac{n_{is}-n_{ic}}{n_{ic}}\right)^2} \times 100\% \qquad (2)$$

where N denotes the total number of selected species in the simplified chemistry; n_{ic} denotes the number density of the ith selected species obtained using the more complete chemistry; and n_{is} denotes the number density of the ith selected species obtained using the simplified chemistry. The calculated results show that the RMSE of the selected species is strikingly less than 1.8%, and the computation time is reduced by a factor of 2.1 using the Simplified Chemistry 2 compared with that using the more complete chemistry. The computational efficiency is improved because the numbers of species and reactions are reduced dramatically. In addition, the current densities and all the densities of the charged, excited and neutral species using the Simplified Chemistry 1 and 2 are both in excellent agreement with the current densities using the more complete chemistry. Thus, the Simplified Chemistry 1 and 2 are both able to capture the change in the density of the selected species as a function of the ammonia concentration with an error that could be ignored in practice. Finally, the Simplified Chemistry 2 is chosen as the reduced chemical kinetics for modeling the $N_2/O_2/NH_3$ AP-DBD because of its better accuracy and acceptable computational time.

4. Conclusion

In this study, we numerically investigated the mechanisms of light emission (NO-γ, NO-β and N_2-SPS) in a planar N_2/NH_3 AP-DBD and included the effects of oxygen impurities using a self-consistent 1D fluid model. The simulated results were validated by their agreement with the OES measurements in the trends due to the change in ammonia addition. The results show that all of the emission intensities decrease as NH_3 increases. The decrease in the N_2-SPS line intensity is caused by electrons binding to NH_3, which weakens the direct electron-impact excitation. The decrease in the NO-γ line intensity is caused by decreases in the amounts of $N_2(A)$ and NO(A), and the decrease in the NO-β line intensity is caused by decreases in both N and O. The simulated results show that the discharges are typical Townsend-like discharges with nitrogen having oxygen impurities with ammonia addition ranging from 0% to 1%. The power absorbed by the ions for

the N_2/O_2 DBD is smaller compared with that for the N_2/O_2 DBD with a small amount of ammonia addition because N_2^+ and N_4^+ are exchanged with NH_3 indirectly and effectively to form NH_4^+, which is lighter than N_2^+ and N_4^+. The simulated results show that the amount of atomic oxygen decreases rapidly with increasing ammonia addition, which leads to less etching on PLA surfaces, and the simulated results agree with the experimental observations [2]. The reduced chemical kinetics is justified by the good agreement of the simulation results with the results obtained using the more complete chemical kinetics. The complete chemistry, including 48 species and 235 reactions, is reduced to 33 species and 87 reactions with only slight deviation in the simulation results. With the choice of this set of reduced chemical kinetics, the computational time decreases 2.1 times in the 1D fluid modeling with essentially the same electrical properties and less than 1.8% root mean squared error for the selected species compared with that using the more complete chemistry, when oxygen (impurity) is fixed at 30 ppm and ammonia varies in the range from 0% to 1%. This Simplified Chemistry 2 is currently applied using a parallel fluid modeling code [26] with a gas flow solver [27] for the simulation of a practical two-dimensional $N_2/O_2/NH_3$ AP-DBD jet. One could expect it to save an appreciable amount of computational time, for which the results will be reported elsewhere in the near future.

Acknowledgments

The authors are highly grateful for the financial support of the National Science Council of Taiwan through the grant NSC-101-2221-E-009-041-MY3, and the computing resources provided by the National Center for High-performance Computing of Taiwan throughout the study performed in this paper.

References

[1] Yang Y W, Kuo C L, Wen C C, Wu J Y, Huang H Y, Chiang M H and Wu J S 2011 Paper presented at the *8th Int. Conf. on Flow Dynamics (Sendai, Japan)*
[2] Yang Y W, Wu J Y, Liu C T, Liao G C, Huang H Y, Hsu R Q, Chiang M H and Wu J S 2013 *J. Biomed. Mater. Res.* A at press (doi:10.1002/jbm.a.34681)
[3] Klages C P and Grishin A 2008 *Plasma Process. Polym.* **5** 368
[4] Li F L, Lin K M, Yang Y W, Hung C T, Wu J S and Yu J P 2012 *Plasma Chem. Plasma Process.* **32** 547
[5] Androulakis I P 2000 *AIChE J.* **46** 361
[6] Kee R J *et al* 2007 *CHEMKIN* Release 4.1.1, Reaction Design, San Diego, CA
[7] Lin K M, Hung C T, Hwang F N, Smith M R, Yang Y W and Wu J S 2012 *Comput. Phys. Commun.* **183** 1225
[8] BOLSIG$^+$ www.bolsig.laplace.univ-tlse.fr
[9] Ellis H W, Pai R Y, McDaniel E W, Mason E A and Viehland L A 1976 *At. Data Nucl. Data Tables* **17** 177
[10] Ellis H W, McDaniel E W, Albritton D L, Viehland L A, Lin S L and Mason E A 1978 *At. Data Nucl. Data Tables* **22** 179
[11] Tochikubo F, Uchida S, Yasui H and Sato K 2009 *Japan. J. Appl. Phys.* **48** 076507
[12] Bird R B, Stewart W E and Lightfoot E N 2007 *Transport Phenomena* (New York: Wiley) p 525
[13] Gherardi N, Gat E, Massines F, Lemoing S and Ségur P 2001 *Proc 15th Int. Symp. on Plasma Chemistry (Orleans, France)* vol 1, p 97
[14] Chiang M H, Liao K C, Lin I M, Lu C C, Huang H Y, Kuo C L, Wu J S, Hsu C C and Chen S H 2010 *Plasma Chem. Plasma Process.* **30** 553
[15] Brandenburg R, Maiorov V A, Golubovskii Y B, Wagner H E, Behnke J and Behnke J F 2005 *J. Phys. D: Appl. Phys.* **38** 2187
[16] Fateev A, Leipold F, Kusano Y, Stenum B, Tsakadze E and Bindslev H 2005 *Plasma Process. Polym.* **2** 193
[17] Cheng K W, Hung C T, Lin K M, Chiu Y M, Wu J S and Yu J P 2012 *Japan. J. Appl. Phys.* **51** 116001
[18] Arakoni R A, Bhoj A N and Kushner M J 2007 *J. Phys. D: Appl. Phys.* **40** 2476
[19] Moravej M, Yang X, Hicks R F, Penelon J and Babayan S E 2006 *J. Appl. Phys.* **99** 093305
[20] Choi Y, Kim J and Hwang Y 2006 *Thin Solid Films* **506** 389
[21] Massines F, Ségur P, Gherardi N, Khamphan C and Ricard A 2003 *Surf. Coat. Technol.* **175** 8
[22] Massines F, Gouda G, Gherardi N, Duran M and Croquesel E 2001 *Plasmas Polym.* **6** 35
[23] Wagner H E, Brandenburg R, Kozlov K V, Morozov A M and Michel P 2005 *Contrib. Plasma Phys.* **45** 338
[24] Rabitz H, Kramer M and Dacol D 1983 *Annu. Rev. Phys. Chem.* **34** 419
[25] Saltelli A, Ratto M, Tarantola S and Campolongo F 2005 *Chem. Rev.* **105** 2811
[26] Lin K M, Hu M H, Hung C T, Wu J S, Hwang F N, Chen Y S and Cheng G 2012 *Comput. Phys. Commun.* **183** 2550
[27] Hu M H, Wu J S and Chen Y S 2011 *Comput. Fluids* **45** 241
[28] Li F L, Yang Y W, Lin K M and Wu J S 2012 Paper presented at the *9th Int. Conf. on Flow Dynamics (Sendai, Japan)*
[29] Mao M and Bogaerts A 2010 *J. Phys. D: Appl. Phys.* **43** 205201
[30] Liu D X 2010 *Plasma Sources Sci. Technol.* **19** 025018
[31] Hayashi M 1990 *Nonequilibrium Processes in Partially Ionized Gases* ed M Capitelli and J Bardley (New York: Plenum) pp 333–40
[32] Mätzing H 2007 *Chemical Kinetics of Flue Gas Cleaning by Irradiation with Electrons* (*Advances in Chemical Physics* vol 80) ed I Prigogine and S A Rice (New York: Wiley)
[33] Tatarova E *et al* 2010 *J. Appl. Phys.* **108** 123305
[34] Gordiets B, Ferreira C M, Pinheiro M J and Ricard A 1998 *Plasma Sources Sci. Technol.* **7** 363
[35] Smith D, Adams N G and Miller T M 1978 *J. Chem. Phys.* **69** 308
[36] Dorai R and Kushner M J 2003 *J. Phys. D: Appl. Phys.* **36** 666
[37] Tochikubo F 2002 *Japan. J. Appl. Phys.* **41** 844
[38] Kossyi I A, Kostinsky A Y, Matveyev A A and Silakov V P 1992 *Plasma Sources Sci. Technol.* **1** 207
[39] Panousis E, Ricard A, Loiseau J F, Clement F and Held B 2009 *J. Phys. D: Appl. Phys.* **42** 205201
[40] Herron J T 1999 *J. Phys. Chem. Ref. Data* **28** 1453
[41] Mirokin Y and Mallard G 1998 *The NIST Chemical Kinetics Database*
[42] Pintassilgo C D 2005 *J. Phys. D: Appl. Phys.* **38** 417
[43] Bhoj A N and Kushner M J 2008 *Plasma Sources Sci. Technol.* **17** 035025
[44] Capitelli M, Ferreira C M, Gordiets B F and Osipov A I 2001 *Plasma Phys. Control. Fusion* **43** 371
[45] Gadd G E and Slanger T G 1990 *J. Chem. Phys.* **92** 2194